NANOCOMPOSITE FUEL CELLS

by
AHMET DENIZ BENLI

Submitted to the Graduate School of Engineering and Natural Sciences in partial fulfillment of the requirements for the degree of Master of Science

Sabancı University

January 2019

NANOCOMPOSITE FUEL CELLS

APPROVED BY:

Prof. Dr. Mehmet Ali Gülgün
(Thesis Supervisor)

Prof. Dr. Selmiye Alkan Gürsel

Prof. Dr. Sedat Alkoy

DATE OF APPROVAL: 04/01/2019

ABSTRACT

NANOCOMPOSITE FUEL CELLS

AHMET DENIZ BENLI

M.Sc. Dissertation, January 2019

Supervisor: Prof. Dr. Mehmet Ali Gülgün

Keywords: Nanocomposite electrolyte, ionic conductivity, surface charge, fuel cell

The interactions between the components of the nanocomposite fuel cell electrolyte were investigated. Surface charges were thought to be responsible for the differences in the ionic conductivity. The literature claims that ionic transport in hybrid electrolytes does not happen primarily in the solid oxide or the matrix phase but at the interface between them.

The surface charges of oxide particles are dissociating the matrix salt molecules into positive and negative ion complexes. The complex with the opposite charge sticks to the surface of the particles. The counter-ion moves freely under the influence of the electrical field, thus causing fast ionic current. Therefore, it is postulated that by modifying the surface charges one can affect the ionic conductivity.

The strength of surface acidity was manipulated by reduction without significantly changing the chemistry of the oxide material. TiO_2 (Rutile) was selected as the material whose surface charge was altered by reduction. Ionic conductivities were measured by impedance spectrometry. Surface charges were obtained by isoelectric point measurements. The amounts of reduction were measured by thermogravimetric analysis.

Oxides with different surface charges resulted in different ionic conductivities. Sub-stoichiometric oxides had different strength of surface charges that resulted in correlated ionic conductivities. These interactions of surface charges and the ionic conductivities are explained with the help of a developed model for the composite electrolyte.

ÖZET

NANOKOMPOZİT YAKIT HÜCRELERİ

AHMET DENİZ BENLİ

Yüksek Lisans Tezi, Ocak 2019

Tez Danışmanı: Prof. Dr. Mehmet Ali Gülgün

Anahtar Kelimeler: Nanokompozit elektrolit, iyonik iletkenlik, yüzey yükü, yakıt hücresi

Bu çalışmada nanokompozit yakıt hücresi elektrolitinin bileşenleri arasındaki etkileşimler araştırılmıştır. Partiküllerin yüzey yüklerinin iyonik iletkenlik üzerindeki farklılıklardan sorumlu olduğu düşünülmüştür. Literatürde, nanokompozit elektrolitlerde iyonik taşınmanın esas olarak katı oksit veya matris fazlarında değil, fazlar arasındaki arayüzlerde gerçekleştiği belirtilmiştir.

Oksit parçacıklarının yüzey yükleri, matris tuz moleküllerini, pozitif ve negatif iyon komplekslerine ayırmaktadır. Ters yüklü iyonlar, parçacıkların yüzeyine yapışır. Buna karşın karşıt yüklü iyonlar, elektrik alanın etkisi altında serbestçe hareket ederek, hızlı iyonik akıma neden olur. Dolayısıyla, yüzey yüklerini modifiye ederek iyonik iletkenliğin etkileneceği öngörülmüştür.

Malzemenin kimyasını önemli ölçüde değiştirmeden indirgeme deneyleri ile oksit partiküllerin yüzeylerinin asitlik derecesi değiştirilmiştir. TiO_2 (Rutil) yüzey yükü değiştirilen oksit malzeme olarak seçilmiştir. İyonik iletkenlikler empedans spektrometresi ile ölçülmüştür. Yüzey yükleri, izoelektrik nokta ölçümleri ile elde edilmiştir. İndirgeme miktarları, termogravimetrik analiz metodu ile ölçülmüştür.

Farklı yüzey yüklerine sahip oksitler farklı iyonik iletkenliklerin oluşmasına sebep olmuştur. Stokiometrisi değiştirilen oksitler, farklı yüzey yüklerine sahip olmuştur, bu durum ilişkili olarak iyonik iletkenliklerde değişime sebep olmuştur. Yüzey yükleri ve iyonik iletkenlikteki bu etkileşim, kompozit elektrolit için geliştirilmiş bir model yardımıyla açıklanmıştır.

To my mom and grandma…

ACKNOWLEDGMENTS

I would like to thank my supervisor Prof. Dr. Mehmet Ali Gülgün for his valuable support. I learned how to be a researcher from the best. The guidance of him broadened my horizon both in academy and in real life.

I would like to thank my jury members Prof. Dr. Selmiye Alkan Gürsel and Prof. Dr. Sedat Alkoy for their collaboration.

I would like to thank all professors I was working with as a researcher and teaching assistant. I would like to thank Dr. Meltem Sezen for learning the use of FIB microscopy. I am especially grateful to Prof. Dr. Cleva Ow-Yang for her guidance and help.

I appreciate the support of the all members of research group I was working with. For this, I would like to especially thank Dr. Shalima Shawuti and Dr. Gülcan Çorapçıoğlu for their support.

I would like to thank all people that made this thesis worth publishing. I am very grateful to my mother Ülker Karaca and relatives especially Ekin Emek Berber and Ezgi Berber for their endless support. I am lucky that I have special friends that always there for their true and precious help. For this, I would like to thank Şule Ruveyda Turkurka, Cihangir Can, Cem Bahadır Aksoy and Melike Barak.

This study was supported by TUBITAK 1001 grant "Farklı oksit nanoparçacıkların katı tuz matrisindeki iyon ayrıştırıcı özelliklerinin incelenmesi" with project number 114M517.

TABLE OF CONTENTS

LIST OF FIGURES

LIST OF TABLES

LIST OF ABBREVIATIONS

AFC	Alkaline Fuel Cell
BET	Brunauer-Emmett-Teller
DLS	Dynamic Light Scattering
DLVO	Derjaguin-Landau-Verwey-Overbeek
DSC	Differential Scannin Calorimetry
DTA	Differential Thermal Analysis
EDL	Electrical Double Layer
EIS	Electrochemical Impedance Spectroscopy
IEP	Isoelectric Point
LTSOFC	Low Temperature Solid Oxide Fuel Cell
MCFC	Molten Carbonate Fuel Cell
PAFC	Phosphoric Acid Fuel Cell
PEMFC	Polymer Electrolyte Membrane Fuel Cell
PZC	Point of Zero Charge
SDC	Samarium-doped Ceria
SEM	Scanning Electron Microscopy
SOFC	Solid Oxide Fuel Cell
TGA	Thermogravimetric Analysis
XRD	X-ray Diffraction
YSZ	Yttria Stabilized Zirconia

1. INTRODUCTION

1.1. Fuel Cell Overview

Energy industry has gained importance for today's developing world in such a way that it necessitates alternative methods or materials to overcome and improve the current energy problems. Current means of energy conversion systems causes environmental alert in terms of pollution. Global warming has become a dramatic issue such that greenhouse gases in the Earth's atmosphere has risen remarkably in the last century [1].

Fuel cells in this case can be an answer to the demand of new alternatives since they offer a promising route for the use of energy. Fuel cells are defined as electrochemical systems where electrical and thermal energy are obtained from chemical energy supplied by fuels [2]. This technology is an alternative approach for charging the electronic appliances used in houses, automobiles and even some big scale manufacturing plants. Fuel cells have been used not only in large scale vehicles but also in microelectromechanical systems such as remote sensors as energy converters [3]. Fuel cells have an advantage over the use of fossil fuels where CO_2 emissions due to combustion reactions occur. The upside is in terms of clean emission, electrical efficiency and silent operation [4]. Fuel cells have high potential to get high energy efficiencies, lowest possible costs, and applicability to industrial level processes by the developments in the 21st century [1].

There are several fuel cell technologies involving different materials and operating in different temperature ranges. They are composed of two electrodes and an electrolyte that supplies high ionic conduction but also low electronic conduction in order to work efficiently. Fuel cells are classified depending on their electrolyte types which are responsible for ionic conduction. One fuel cell type is solid oxide fuel cells (SOFCs) that also constitute the platform of this study [5]. SOFCs uses diffusion of oxygen ions through a solid electrolyte layer causing ionic conduction. This interaction is fueled by reactions between oxidant and fuel giving electricity [6] [7].

SOFCs are composed of an oxide electrolyte providing ionic conduction. They can operate through a broad temperature range up to 1000 ºC depending on the energy efficiency, type and cost of materials, interconnects and insulation. However, the ultimate aim is to make the working temperature as low as possible. Time effective use and improvement in durability as well as robustness are still needed [5].

1.2. Principles of Fuel Cells

Up until now, there were many approaches to build fuel cells yielding a higher efficiency. The differences lie behind the type of electrolytes that are used to construct fuel cells which in turn affect the choice of electrode materials as well as fuel type (affecting the operating temperatures) [8] [9]. Currently, proton exchange membrane, alkali, molten carbonate, solid oxide and phosphoric acid electrolytes are commonly used electrolytes for fuel cell applications [3] [10] [9].

Fuel cells have three different parts which are responsible for different missions. These components are two electrodes and an electrolyte. Electrodes cover the two sides of the electrolyte thereby supplying fuels or oxidants to the system allowing gas or liquid flow which requires a porous structure. On the contrary, electrolyte should be impermeable to gas diffusion [11].

1.3. Types of Fuel Cells

Classification of fuel cells are done considering electrolyte materials used. Comparison of different fuel cell types in terms of electrolyte, efficiency, operating temperatures, applications, advantages and disadvantages are listed in Table 1.1 [9] [12] [13] [14].

Table 1.1. Comparison of the types of fuel cell [9] [12] [13] [14].

Fuel Cell Type	Common Electrolyte	Operating Temperature	Efficiency	Applications	Advantages	Disadvantages
Polymer Electrolyte Membrane Fuel Cell (PEMFC)	Perfluoro sulfonic acid	40-80 °C	40-50%	-Backup power -Portable power -Distributed generation -Transportation -Specialty vehicles	-Solid electrolyte reduces corrosion and electrolyte management problem -Low temperature -Quick start-up	-Expensive catalysts -Sensitive to fuel impurities -Low temperature waste heat

Alkaline Fuel Cell (AFC)	Aqueous solution of potassium hydroxide soaked in a matrix	65-220 °C	40-70%	-Military -Space	-Cathode reaction faster in alkaline electrolyte, leads to high performance -Low cost components	-Sensitive to CO_2 in fuel and air -Electrolyte management
Phosphoric Acid Fuel Cell (PAFC)	Phosphoric acid soaked in a matrix	205 °C	70%	-Distributed generation	-Higher temperature enables CHP -Increased tolerance to fuel impurities	-Pt catalysts -Long start-up time -Low current and power
Molten Carbonate Fuel Cell (MCFC)	Solution of lithium, sodium, and/ or potassium carbonates, soaked in a matrix	650 °C	60%	-Electric utility -Distributed generation	-High efficiency -Fuel flexibility -Can use variety of catalysts -Suitable for CHP	-High temperature corrosion and breakdown of cell components -Long start up time -Lower power density
Solid Oxide Fuel Cell (SOFC)	Yttria stabilized zirconia	600-1000 °C	70%	-Auxiliary power -Electricity utility -Distributed generation	-High efficiency -Fuel flexibility -Can use a variety of catalysts -Solid electrolyte -Suitable for CHP and CHHP -Hybrid/GT Cycle	-High temperature corrosion and breakdown of cell components -High temperature operation requires long start up time and limits

PEMs have received interest because they are applicable to transport systems. Alkali fuel cells, despite of the fact that they provide high power densities, are not practical due to the necessity of removing the trace CO_2 to avoid formation of non-conducting alkali carbonates. Phosphoric acid fuels are not able to provide high power densities in the applications. Molten carbonate and solid oxide fuel cells are important candidates for the stationary power generation. However, high temperature operation conditions of SOFC decreases the lifetime of the cells.

1.4. Fundamentals of Solid Oxide Fuel Cells

Solid oxide fuel cells (SOFCs) are composed of three essential parts as well as other fuel cell types i.e. two porous electrodes which are anode and cathode and an electrolyte. The electrolyte of an SOFC is a ceramic in order to withstand high operating temperatures (1000 ^{o}C). Electrolyte is responsible for ionic conduction and at the same time it should

be electronically an insulator. On the other hand, cathode and anode components should conduct electrons and they must have a coefficient of thermal expansion which is similar to electrolyte materials. Cathode is the component that is responsible for oxygen anion supply to the electrolyte where reduction of oxygen molecules into oxygen anions occur by electrons coming from external circuit. Equation 1.1 represents the cathodic reaction [15].

$$O_2(g) + 4e^- \rightarrow 2O^{2-} \qquad \text{(Equation 1.1)}$$

Anode is the part where combustion reactions occur by oxygen ions with the help of fuels present at the electrolyte interface and electrons are given to the circuit. Equation 1.2 represents the anodic reaction e.g. combustion reaction by H_2 used as a fuel [15]:

$$H_2(g) + O^{2-} \longrightarrow H_2O(g) + 2e^- \qquad \text{(Equation 1.2)}$$

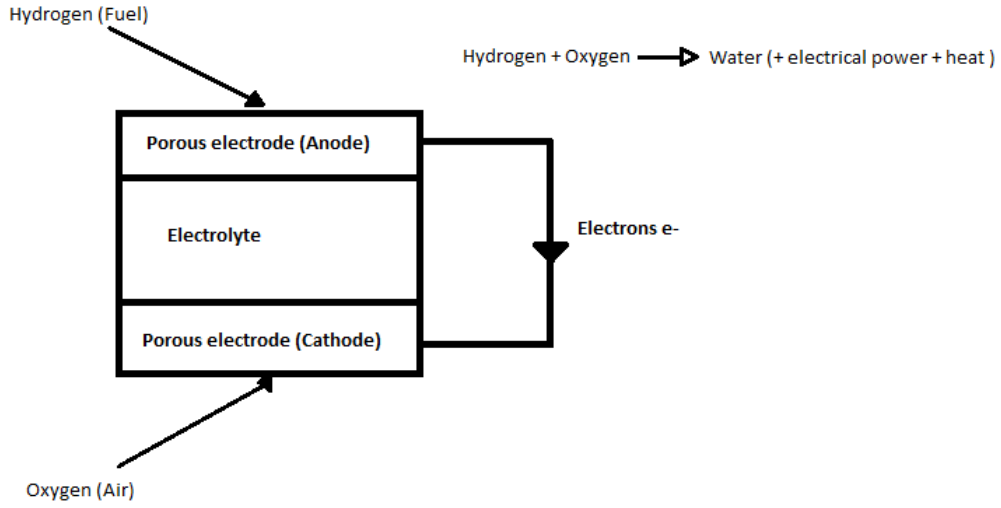

Figure 1.1. Schematic diagram of solid oxide fuel cell (SOFC).

All in all, the oxygen molecules reduced in the porous cathode electrode by taking electrons coming from the circuit hence oxygen ions are formed. These anions are forced to diffuse from cathodic part to anodic part of electrodes via the electrolyte separating them from each other. The driving force for the diffusion is the chemical potential differences between the electrodes. In the anodic electrode, the oxygen ions react with the fuel supplied there, commonly H_2 producing water, H_2O. This combustion reaction

creates electrons thereby completing the external electronic integration of the circuit. As a result, both electricity, heat and water are obtained [16].

1.5. State of the art of Solid Oxide Fuel Cells

Solid oxide fuel cells have a significance in fuel cell industry since they offer advantages such as flexibility in choice of fuel, modular construction, high efficiency and suitability to many applications [17] [18]. Moreover, they have tolerance to carbon monoxide so that purification requirement of fuel is low. Their high tolerance to impurities which are not compatible to other fuel cells and flexibility of the fuel composition cause less requirement of fuel processing and result in ease of application. They do not contain liquid electrolytes which are potentially corrosive and hard to manage [19]. High operating temperature conditions of SOFCs lead to release of heat in addition to electricity. This heat can be integrated into heat and power systems to generate more electricity thereby increasing efficiency [8] [20]. Moreover, high temperature operation of SOFCs give way to conversion of carbon monoxide (CO) into carbon dioxide (CO_2) making environmentally friendly impact.

However, SOFCs have not reached the a wide-spread use commercially. This situation mainly arises from high working temperatures of them, costly materials and shorter lifetime due to high temperatures. Partial electronic conductivity is also an issue for some SOFC types. [18] [21] [22] [23] [24].

The two main objective of studies on the solid oxide fuel cells are to lower the operating temperature and hence the cost, to maintain a high ionic conduction and good performance at lower temperatures [25] [26] [27]. Decrease in operating temperature directly decreases the cost because this give way to use of cheaper components and therefore decreases the cost of replacement. Low temperatures enhance overall system efficiency and causing less thermal stresses in the active ceramic structures. Therefore, the expected lifetime of SOFCs increase [8] [28] [29] [5].

There were many approaches to lower high operating temperatures of SOFCs from 1000 ^{o}C to around 600 ^{o}C without sacrificing the high ionic conduction through the electrolytes [22] [23] [24] [30]. These include thin films, proton conductors, ceria-based materials, carbon nanowires, co-doped approach [22] [23] [24] [30] [25] [26]. Yttria-stabilized zirconia, samarium-doped ceria, gadolinium-doped ceria and lanthanum strontium gallate

magnesia are the examples for the materials used to construct the cells [22] [23] [24] [30]. Another approach to obtain better material properties and performances is combining two material types thereby building nanocomposite electrolytes. The working principles of them is based on dual phase conduction involving oxygen and protons [25] [26] [27] [31].

The nanocomposite or two-phase electrolytes make use of their interfaces and surfaces created by their phases thereby modifying and stabilizing the surface properties [32]. Here, the selection of second phase materials are important since they can affect the interactions between particles as well as phases and can cause an interfacial electric field [32]. It was shown in a recent study that the core-shell ceria-carbonate electrolytes resulted in a successful thermal stability compared to single-phase ceria. The composite structure created a so-called superionic conduction. The addition of second phase materials resulted in modification of the surface energy and change in diffusion rate of the nanostructured materials [27]. It also prevented particle size growth which meant that more interfaces were present for diffusion [32].

For single phase polycrystalline materials, grain boundaries and ion transport activation energy act as barrier for ionic transport causing resistivity at micrometer level [32]. At this level, grain boundaries resist the ionic transport and this resistivity is higher than the grain resistivity. At nano scale, decrease in particle size i.e. increase in the grain boundary area changes this behavior and causes an increase in the concentration of mobile species at grain boundaries [32]. Therefore, with the use of nano-sized particles in single-phase materials, ionic conductivity increases due to the ionic regions. However, certain nano-sized single phase materials are not stable at high operating temperatures and electronic conductivity instead of ionic conductivity become dominant [33][32]. Nanocomposite making in that respect can be a promising approach to overcome this problem providing interfaces for ionic conduction [32]. For nanocomposites, at low temperatures which are defined as 300-600 ^{o}C, ionic conduction or superionic conduction is a result of interfaces present in the nanocomposites. Interfaces are discontinuities which interrupts the symmetry of matrix [34]. At the region close to interfaces, there exist a charged region i.e. so-called space charge zone inside the particle which is thermodynamically favorable whereas the bulk is electronically neutral [35]. Ionic diffusion predominantly takes place in these interfaces since the defect concentrations are accumulated there resulting in highly mobile ions and higher ionic diffusivity than that of the bulk. For example, covering boundaries of a phase with a surface active second phase, like the case in ceria-

based composite electrolytes, is a way to do so [36] where interfaces are responsible for high ionic conduction [32]. The secondary phases in nanocomposites make it possible to suppress the growth of nanoparticles as well. Covering the nanoparticles with a second phase forms a nano-core and nano-layer-shell structure resulting from the interaction between phases of nanocomposite. By this way, nanoparticles do not suffer from the energetic growth at high temperatures but instead the interactions between constituent phases can exhibit new properties at their interfaces [32]. Therefore, with the presence of a second phase in two-phase materials, interfaces and surfaces with new properties are obtained and also by means of a second phase, the surface properties can be stabilized and modified [32]. In literature, it was reported that using the core-shell ceria-carbonate nanocomposites showed outstanding properties in terms of thermal stability compared to single-phase ceria [27] [37] In addition, superionic conduction were obtained by modifying the surface energy and improving the diffusion rate of ions in nanocomposites with the use of second phase materials [32].

As mentioned, there is a need for combining different materials hence different properties giving rise to the ionic conductivity of fuel cell electrolytes. Therefore, in this study it was decided to focus on nanocomposite solid oxide fuel cells to get better properties resulting in better performances.

1.6. Nanocomposite Electrolytes for Solid Oxide Fuel Cells

Nanocomposite electrolytes are composed of oxide nanoparticles and amorphous salt phases. These composite electrolytes studied operate with high ionic conduction efficiency via the interaction of oxide nanoparticles and the amorphous salt matrix. It was seen that this interaction improves the ionic conduction of electrolytes [38]. The mechanism behind this behavior was explained as oxide nanoparticles causing dissociation of salt molecules into their components [38].

It was stated that interface regions between oxide and carbonate phases resulted in improved ionic conductivities in the case, SDC and Na_2CO_3 combined together to form composites. There is ionic conduction through the electrolyte by H^+ and O^{2-} diffusion therefore facilitating a dual conduction approach in the nanocomposite [39].

In this study we focused on nanocomposite electrolytes and their working mechanism as discussed in detail in next chapters. The interaction of oxide nanoparticles with the

amorphous salt matrix causes a change in the ionic conductivity of the nanocomposite eventually. On the cathodic side, the system is fed with oxygen. Oxygen molecules are split into its atoms thereby getting electrons coming from the outside circuit to be ionized. These oxygen ions are transported from cathode to the anodic side through the electrolyte that is composed of solid oxide and carbonate phases. When they reach to anode electrode, the condition results in a reaction between hydrogen gas and oxygen ions forming water, H_2O. At the same time, oxygen ions at the cathodic side combine themselves with CO_2 gas forming CO_3^{2-} ions. CO_3^{2-} ions also diffuses through the electrolyte carrying -2 charges. At the anodic side, CO_3^{2-} ions give off their oxygen contributing ionization of hydrogen and water formation leaving behind CO_2. The produced CO_2 gas is fed back to the cathodic side for the gas supply through an outside bypass duct. The electron release after ionization of hydrogen molecule is supplied to the external circuit. This cycle creates an electrical current and the electrons are carried to the cathodic side. Hydrogen ions produced at the anode diffuse to the cathodic side via electrolyte and they combine with oxygen ions to form water there. The complete system operates with the principle of mobile ions as it can be seen in Figure 1.2 as well.

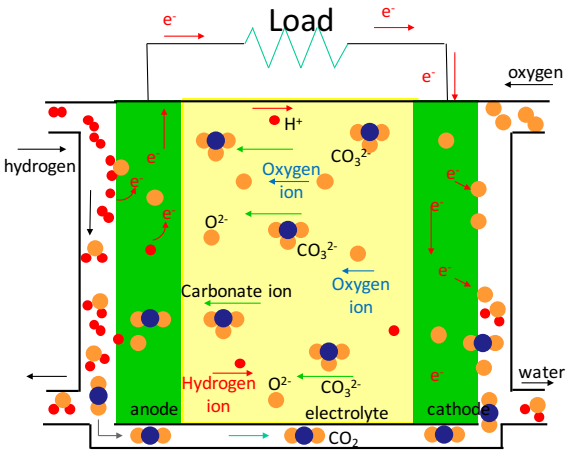

Figure 1.2. Schematic diagram of nanocomposite fuel cells.

Cathode is the component that is responsible for oxygen and carbonate anion supply to the electrolyte by means of reduction with electrons coming from external circuit. Equation 1.3 and 1.4 represent the reaction in cathode electrode:

$$O_2(g) + 4e^- \rightarrow 2O^{2-} \quad \text{(Equation 1.3)}$$

$$CO_2(g) + O^{2-} \rightarrow {CO_3}^{2-} \quad \text{(Equation 1.4)}$$

At anode, carbon dioxide formation, ionization of hydrogen and water formation are observed thereby giving electrons to the circuit. Equation 1.5, 1.6 and 1.7 represent the anodic reactions:

$${CO_3}^{2-} \rightarrow CO_2(g) + O^{2-} \quad \text{(Equation 1.5)}$$

$$H_2(g) \longrightarrow 2H^+ + 2e^- \quad \text{(Equation 1.6)}$$

$$H_2(g) + O^{2-} \longrightarrow H_2O(g) + 2e^- \quad \text{(Equation 1.7)}$$

1.7. Ionic Conduction and Nanocomposite Effect

Certain high ionic conductivity electrolytes of solid oxide fuel cells have few drawbacks: when the operation of solid oxide phase is performed under reducing atmospheres additional electronic defects are formed. An example to this is seen in cerium oxide electrolytes where ceria powders were reduced under H_2 passage conditions. The electronic conductivity instead of ionic conductivity in the electrolyte increases by reduction which results in deterioration of overall cell voltage. [40] This problem can be overcome by the approach of nanocomposite making for the electrolytes with the use of solid oxide and alkali salt matrix as in the example of ceria-based solid oxides and carbonates [41] [42] [43] [44] [45] [46].

In literature it was reported that solid oxide phase acts as a scaffold for carbonate phase in order for the electrolyte to operate at intermediate temperatures in between 400 to 650 ^oC. These phases together contribute to the overall electrolyte performance remaining as stable phases [26]. The nanocomposite electrolytes studied in the literature gave ionic

conductivity values of 0.1 S/cm between 400 to 600 ºC by the diffusion of ions in the superionic pathways [32].

The ionic conduction mechanism in nanocomposites was explained in the earlier studies of Shawuti and Gulgun. The model proposed by Shawuti and Gulgun in the interaction of particle size and amount with ionic conductivity of nanocomposites indicates that the matrix phase i.e. carbonate molecules are attracted by the surfaces of solid oxide nanoparticles [38]. The salt molecules of matrix phase (carbonates) dissociate thereby creating freed counter ions. These counter ions are concentrated around the surfaces of solid oxide particles giving a shell form. These solid oxide particles having concentrated counter ions around their surfaces create interconnected paths for the counter ions to percolate through the matrix. These interconnected ways are considered as superionic conduction regions for ions to move in nanocomposite electrolyte. The schematic illustration of this system can be seen in Figure 1.4 below.

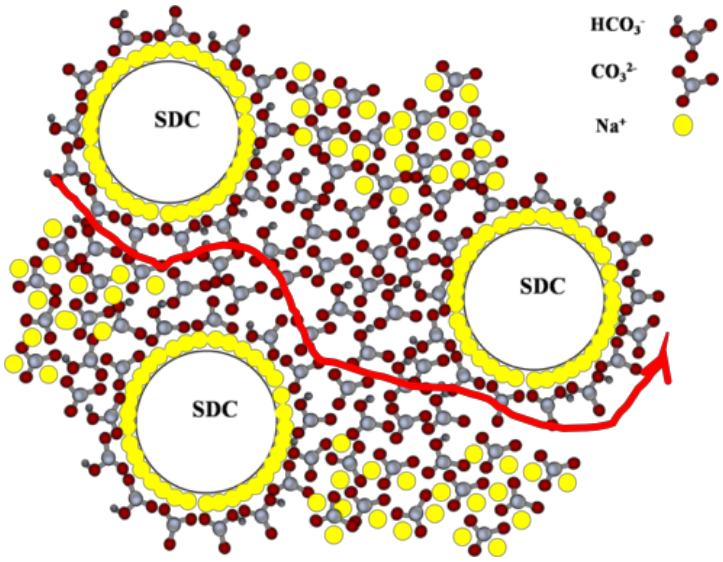

Figure 1.3. Schematic illustration of superionic paths of SDC-carbonate nanocomposite [38].

1.8. Ionic Conductivity and Particle Size Effect

Nanocomposites that are used for electrolytes of low temperature SOFCs (LTSOFCs) have significant advantages because of the nanoparticles they include. Any change and influence on physical and chemical properties of nanoparticles have an impact on the overall properties and performances of the fuel cells. This impact can be an improvement

as well as an appearance of a new property. The size of particles in that sense is an important aspect to consider for ionic conduction. Surface properties of particles gain significance with the decrease in particle sizes. Smaller particles provide superionic conduction surfaces.

The earlier studied ionic conductivity values of nanocomposites in the literature already gave very promising results for ceria and salt two phase nanocomposite. The reported ionic conductivity value for ceria-based composites were seen in 10^{-2} to 1 S/cm range at intermediate temperatures 400-600^{o}C [25]. Later in the literature, the ionic conductivity of higher than 0.1 S/cm was obtained in temperature scale between 300 and 600 ^{o}C for two phase nanocomposites. This notable value signifies the importance of interfaces as superionic conduction highways in a continuous network [47].

Another study performed on nanocomposites showed the encouraging effect of smaller particle sizes of solid oxide phases on ionic conductivity by investigating the percolation behavior of two phases. It was seen that as the particles size gets smaller, the ionic conductivity gets better. This is because of the fact that specific surface area of particles become larger as the particles get smaller which in turn leads to the accumulation of high amount of freed counter ions around these surface layers [48]. The freed counter ions can be introduced to a superionic conduction path percolating through the surface layers carrying charges by interaction of solid oxide and salt phases in the nanocomposite electrolytes [49].

1.9. Soggy-Sand Electrolytes

The ionic conductivity improvements with the interaction of solid oxide and salt matrix phases in nanocomposite electrolytes operates with the same principle with colloidal or so called soggy-sand electrolytes. Soggy-sand electrolytes are composite electrolytes which contain nano-crystalline solid and (amorphous) liquid phases [50] [51]. These phases have synergistic electrical properties affecting the overall electrolyte performance. These electrolytes contain a great number of choices of several parameters i.e. degrees of freedom such as solvent, salt and filler type as well as their grain size, volume fraction

and surface chemistry. Therefore, mechanical and electrical characteristics of soggy-sand electrolytes can be manipulated easily [52].

An example comes from the electrolytes used in Li ion batteries. Soggy-sand electrolytes improves Li^+ ionic conductivity thereby providing a matching mechanical behavior desirable for the material. It means that the electrolyte body has a consistency similar to a solid and it is also suitable to cover the contact surfaces of electrodes [52]. Another research performed on multi-phase electrolytes revealed that using solid-solid composites composed of insulating oxides and weakly cation conducting crystalline solids improved the ionic conduction considerably (Al_2O_3 as insulating solid oxide and Li-, Ag- and Tl-halides as the other phase) [53] [54] [55] [56] [57] [58] [59] [60].

When the γ-Al_2O_3 is used as filler phase, an ionic conductivity for cation up to several orders of magnitude could be obtained at room temperature specially for mesoporous materials. In other words, the ionic conductivity was the result of Li^+, Ag^+ and Tl^+ cation adsorption in the surface of Al_2O_3 phase thereby causing vacancy formation in halide [61] [62]. Also, anion vacancy conductivity was observed in the composites by anion adsorption in the surfaces of oxide phases. An example for this case was reported for CaF_2-SiO_2 and PbF_2-SiO_2 composites where improved ionic conductivity occurred by F^- anion vacancies [63] [64] [65] [66] [67].

In Soggy-sand electrolytes where the matrix is salt containing solvent and oxide is the filler phase, the increase in concentration of ions around the filler particles leads to an improvement in ionic conductivity [52]. Therefore, ionic conduction of soggy-sands happens predominantly in amorphous salt matrix regions around the particles. The amorphous phase was shown to have 10^4 times higher ionic conductivity than crystalline filler phase [50] [51]. On the other hand, for the materials composed of pure Na_2CO_3 phase, ionic conductivity values were in between 10^{-5} and 10^{-4} S/cm at temperature range of 500-580 ^oC being quite lower than the ionic conductivity values of nanocomposites (SDC-Na_2CO_3) given in the literature where the oxide particles are dispersed in amorphous salt matrix [39] [68].

The difference between ionic conductivity values of pure Na_2CO_3 and SDC-Na_2CO_3 nanocomposites is the presence of interfaces as well as the amorphous nature of Na_2CO_3 [49]. Increasing temperatures leads to an increase in the disorder of Na_2CO_3 phase due to

its amorphous nature. This results in better protection of SDC surface and an increase in oxygen ion diffusion in interfaces [68]. Increasing disorder or the amount of amorphous phase means that structure become much more open which positively affect the ionic conductivity. Amorphous nature of Na_2CO_3 was observed in the studies of Shawuti and Gulgun. In nanocomposites made up of SDC and Na_2CO_3 phases, diffraction peaks of crystalline Na_2CO_3 were not present in XRD analyses results but instead SDC crystal peaks were there. However, the diffraction peaks belong to the crystalline structure were found in as received and heat treated Na_2CO_3 powders. DSC analyses also supported this result. Glass-transition type structural relaxation of Na_2CO_3 was observed supporting the amorphous structure of Na_2CO_3 phase [38].

1.10. Composite Electrolyte and the Effect of Surface Charge

Colloidal suspensions, soggy-sands and nanocomposites are types of composite electrolytes in which similar or same mechanism is responsible for ionic conductivity. This mechanism is based on the relation of the surface charges of the particles with the amorphous matrix and its interaction in the electrolyte. Surface ions i.e. surface charge interaction with the counter ions can be understood by studying electrical double layer (EDL) topic presented in Figure 1.4 below.

Particles with surface charges causes electrostatic forces in the liquid matrix affecting the colloidal stability [69]. There exists van der Waals forces (attractive) and repulsive electrostatic forces between particles in the liquid which was explained by Derjaguin-Landau-Verwey-Overbeek (DLVO) theory [70]. The theory states that dispersion should be dilute, and the dispersed particles have Brownian motion in the liquid. For the particles at a small distance in a solution, van der Waals forces (attractive) are effective and the stability of the particles is sustained by repulsive electrostatic forces to prevent coagulation or instability in a colloidal dispersion [69].

The electrical double layer describes the interaction of ions in solution with the surface of the particles. This interaction forms a nonuniform dispersion of ions from the surfaces of particles to the bulk [71]. This distribution is due to the attractions of counter ions and the repulsions of co-ions which can be seen in the figure 1.4. For a colloidal particle with surface excess charges, counterions are attached to the surface of the particles, wherein ions with the same charge are repelled, and these charge interactions provide the

electroneutrality at the interfaces of solid and liquid phases [69]. This creates a potential difference between surface of particles and the bulk. In that respect, zeta potential determines the distribution of ions and counter ions in the solution. The existence of ions around the surfaces of particles causes the interfacial ionic transport [69] [71]. This is because there will be a region of "co-ions" surrounding surface attached counter ions and these (mobile) "co-ions" are the reason of the ionic transport in nanocomposite electrolytes. Therefore, the electrical double layer knowhow gives a good explanation about the stability of colloidal suspensions considering both mobility and the charges of ions around the particles. These studies are performed by zeta potential measurements because there is a surface potential between solid particles and liquid or the matrix due to the appearance of surface charges in interfaces of two phases of electrolyte [72].

In figure 1.4 the distribution of ions around a charged particle is shown. There are three layers named as inner and outer Helmholtz layers and a diffuse layer. Stern plane is the layer between inner and outer Helmholtz planes and there is a linear charge and potential distribution at this plane. The slipping plane is the layer, which separates the immobile surface attached ions and mobile ions in the solution. It is located in the diffuse layer giving to a zeta potential [69].

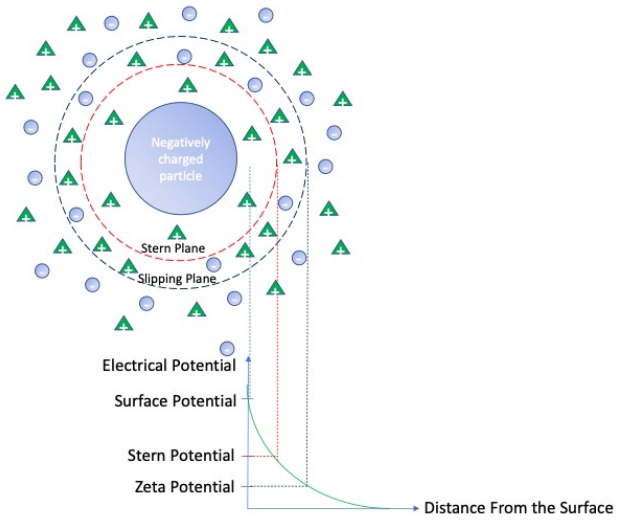

Figure 1.4. Electrical double layer which explains surface charge effect in composite electrolytes.

The improvement in ionic conductivity resulted by the increase in concentration of ions around the filler particles can be explained by two mechanisms. First, it is assumed that

there is an adsorption force where the counter ions are concentrated around the surfaces of filler particles. Second, there is an equilibrium between association and dissociation mechanism of ions [52]. As a result of the equilibrium of these mechanisms, counter ions are attached to the surfaces of particles and the co-ions become mobile. Therefore, it is important to consider the surface charges around the particles. This is because they give practical understanding about the mobility, adsorption and the stability of ions and also surface acidity and basicity of particles. These terms are quite important to understand the behavior of surface adsorbed ions and the corresponding effect on counter ions. As a result, electro-kinetic studies are performed. In that respect, point of zero charge (PZC) that is the term for zero electrical charge density on the surface of particles gain significance. Point of zero charge is the point that no net charge is present at the surface of particle which is defined by its pH value in the solution [73]. For example, in order to increase the cation mobility, solid oxide (filler) particle should have an acidic surface behavior. It can be useful to consider point of zero charge of solid oxides for instance SiO_2, TiO_2 or ZrO_2 suspensions in water where a detailed surface chemistry should be studied. [52]. There exists an interaction between solid particles and matrix such that surface charges of the solid particles affect the ions in the matrix. Therefore, this mechanism creates an impact to dissociate the ions of salt matrix which correspondingly results in attaching one type of ions to the surfaces of solid particles. These surface adsorbed ions are the ions coming from salt matrix in other words they are oppositely charged compared to the surface of particles. The surface adsorbed ions around the solid particles attract their counter ions (oppositely charged with respect to the adsorbed ions) around this region. In the model suggested by Shawuti and Gulgun, it was stated that the surface of the SDC particles caused Na_2CO_3 salt molecules to dissociate into their components. These dissociated ions are attached to the surface of SDC particles. The remaining counter ions become liberated and mobile, and hence an improved ionic conduction occurs through the interfaces around the particles. [38].

As it was mentioned already the particle sizes have a crucial effect on ionic conductivity. Therefore, surface charges are also affected by solid particle sizes which will be also mentioned in the discussion section in this study [74].

In reality, the defect structure of grains influences surface charges. The explanation of this mechanism can be given by looking at grain boundaries. A high ionic conduction in space charge zones near grain boundaries is spotted due to high amount of defect

concentration in these regions. When compared, the bulk itself has low ionic conduction where the defect concentrations are very low [75]. This is associated with the differences in formation energies of defects. With this, there will be an accumulation for the ions on the surfaces (grain boundaries) which shows a difference in terms of the concentrations of ions compared with those in the bulk. Therefore, those surfaces become charged surfaces and can be redistributed within the bulk. Charged surfaces (grain boundaries) lead to a change in the layer nearby the grain boundaries inside the grains. This is determined by space charge layer [76]. The effect of surface charge also describes the ionic conductivity of composite electrolytes depending on the interface regions formed in between two phases [77].

1.11. Objectives of This Research

Soggy-sand electrolytes and their surface charge effect on ionic conductivity gave inspiration for this study. In soggy-sand systems as well as nanocomposites, the operating mechanism for modifying ionic conductivity was assumed to be similar. Commonly, one ion type attaches to the surface of solid particles by adsorption and this creates freeing of counter ions in the region outside zeta potential surface but close to interfaces between phases. Therefore, it was considered to be possible to influence the mobile counter ions in the vicinity of solid particles by changing surface charges. The approach of modification of surface charges was performed by forming defect states in the structure of solid particles [76]. Modified surface charges introduced by defected structures influence the extent of dissociation of matrix salt molecules. Therefore, the study focuses on the interactions of solid oxide particles with amorphous salt matrix in nanocomposite electrolytes and corresponding modification in their ionic conductivity which can be triggered intentionally by forming defects in the solid oxide phase [78] [79].The variation in ionic conductivity of nanocomposite electrolytes were investigated in this study maintaining the use of base oxide material identical. To do so, defect structures of solid oxide particles were altered by reduction at different temperatures and under the passage of reducing gases. This approach made it easier to minimize the chemistry difference. Rutile (TiO_2) was selected as solid oxide particles to be reduced in a tube furnace because of its high tendency to accommodate oxygen vacancy defects under reducing conditions [80].

2. EXPERIMENTAL

2.1. Materials

Rutile, TiO_2, (Aldrich, Germany) had a particle size less than 5 μm. Graphite (Fluka, Germany) powders with a particle size of 1-2 μm was used. Anhydrous sodium carbonate, Na_2CO_3, (Aldrich, Germany) powder was ≥99.5% pure. Deionized water (>18 MΩcm, Millipore Milli-Q) was used in rinsing and solution preparation steps. Varigon gas (Ar + H_2 < 4%). was used for reduction experiments. Flash dry silver paste was used to make conducting contact to the composite pellets (SPI Supplies, West Chester, USA).

2.2. Fabrication Techniques

2.2.1. Preparation of Fine Powders and Reduction Experiments

TiO_2 (initial particle size less than 5 μm) was ground by hand in an agate mortar. TiO_2, Rutile, was left under the passage of reducing gases at different temperatures for reduction in Protherm tube furnace (ALSER, Ankara, Turkey). TiO_2 particles were placed in an Al_2O_3 crucible and placed inside a tube furnace. They were reduced at specified temperatures ranging between 700 ^oC and 1000 ^oC. In addition, one more experiment was performed by placing graphite powder next to rutile powders leaving them under a strongly reducing condition. Graphite powders easily react with oxygen ions. So, the purpose of the addition of graphite powders to the system was to obtain a much better reducing atmosphere due to its oxidation tendency.

2.2.2. Preparation of Fine Powder Mixtures and Composites

Ball milling is a technique that is used to obtain fine powders by grinding them [81]. Ball milling yields reduction in particle size, morphology change of particles, mixing, blending and production of nanocomposites [82]. Ball milling was performed by filling powders and balls up to a certain level which composes approximately ¼ of the total volume of container and letting them mixed by rotating around the horizontal axis. The schematic of ball milling can be seen in Figure 2.1 below.

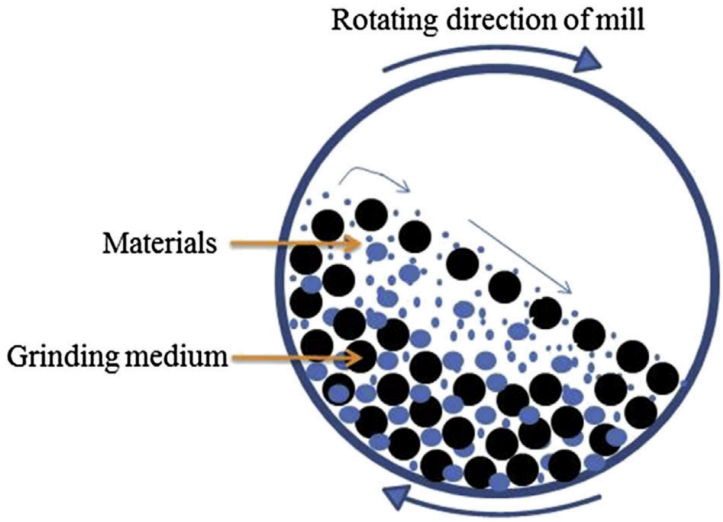

Figure 2.1. Schematic illustration of ball milling process [83].

Rutile, TiO_2, powders were mixed with sodium carbonate (Na_2CO_3) powders with a weight ratio of 90%TiO_2-10%Na_2CO_3 in order to make composites (both for as received and reduced TiO_2 powders). Then, the mixtures were added into HDPE bottles filling them with 1-1.5 grams of powder mixture and by adding yttria stabilized zirconia balls (YSZ), which were 3 mm in diameter and have 1:1 volume ratio with the powder mixture, they were dry-milled for 6 hours to have a homogeneous powder mixture. The milled powders were collected and re-ground by hand in an agate mortar. The powder mixtures (0.5 grams for each pellet) were poured into a mold and pressed under 39 MPa uniaxially to produce pellets (composites) having diameter of 10 mm and thickness of 1 mm. The pressed powder pellets i.e. green compacts were covered with a rubber protection and placed inside a mold filled with technical oil suitable for isostatic pressing. There, they were pressed with 245 MPa to get pellets having less porosity. The pellets were subjected to heat treatments at 700 ^oC in air for 1 hour with a heating rate of 5 ^oC/min to densify i.e. to obtain much less porosity and increasing the strength of pellets. This was done by removal of moisture which appears in as received Na_2CO_3. It means that there will not be further re-oxidation at that temperature through the structure. Then, silver paste was applied to their cross-sectional surfaces after sintering at 700 ^oC for 1 hour. The composite pellet preparation procedure was applied to reduced TiO_2 powders as well.

2.3. Characterization Methods

Composites were produced by as received and reduced TiO_2 powders. TiO_2 powders were combined with Na_2CO_3 powders to sustain 90 wt% and 10 wt% of the total weight of mixture, respectively. The composites were sintered by heat treatment and were characterized by scanning electron microscopy (SEM) and electrochemical impedance spectroscopy (EIS).

As received TiO_2 and reduced TiO_2 powder materials were characterized by x-ray diffraction (XRD), scanning electron microscopy (SEM), thermogravimetric and differential thermal analyses (TGA & DTA), Brunauer-Emmett-Teller (BET) surface area measurements, dynamic light scattering (DLS), isoelectric point (IEP) measurements and auto-titration.

2.4. Heat Treatment

Heat treatment was performed to pellets with a heating rate was settled as 5 ^oC/mins to reach 700 ^oC and wait for 1 hour. The purpose of heat treatment was to get a dense material as well as removal of moisture. In the atmospheric conditions, as received Na_2CO_3 have tendency to become hydrated to form $NaHCO_3.H_2O$. With heat treatment, monohydrate water was removed [38].

2.5. Scanning Electron Microscopy (SEM)

Scanning electron microscopy gives information regarding morphology, particle size, chemical composition and topography of the region at the surface and 1 μm layer beneath the surface [84]. Powders and composites were analyzed under a field emission scanning electron microscope (Zeiss Leo Supra 35, Oberkochen, Germany). TiO_2 Rutile powders were first reduced in a tube furnace at different temperatures. Then, morphology and particle sizes of as received and reduced powders were determined under SEM. Composite pellets were made by combining as received TiO_2 and reduced TiO_2 powders with sodium carbonate (Na_2CO_3) powders. Surface morphology, particle size and distribution of two phases in pellets were measured by SEM. In both cases, the samples were stuck with two-sided carbon tapes onto the surface of stubs to get better electrical conductivity for better SEM images.

2.6. X-Ray Diffraction (XRD)

X-rays are photons having energies in between 100 eV to 100 keV i.e. wavelength from 0.01 to 10 nm. X-ray crystallography method clarifies crystalline atomic structures and phases by diffraction of incident beams of x-rays in many directions. Therefore, density of electrons in crystal can be mapped which in turn gives crystallographic information such as the position of the atoms inside the crystal unit cell, lattice parameter, structure, bonding type, crystalline phases [85].

Powder specimens were measured for their crystal structure and phase distribution analyses with X-ray diffraction (Bruker AXS-D8, Karlsruhe, Germany). They were analyzed with specified settings at 40 kV and 40 mA with Cu Kα radiation (λ=1.5418 Å) with 0.02^{o} as step size and 1 second as data collection time. The 2 theta ranges covered were in between 5^{o} to 90^{o}.

2.7. Thermogravimetric Analysis and Differential Thermal Analysis (TGA & DTA)

Thermogravimetric analysis is a measurement technique responsible for change in mass of a material depending on temperature change or time [86]. Thermal stability; dehydration, decomposition, desorption, and oxidation temperatures and composition of materials can be determined by this technique.

As received TiO_2, rutile, powders and TiO_2 powders that had been reduced at different temperatures and times (at 700, 800, 850, 900, 1000 ^{o}C for 0.5 and 4 hours) were thermally analyzed in air atmosphere from room temperature to 1400 ^{o}C by thermogravimetric analysis (Shimadzu DTG-60H). To do so, powders were placed in sample holder and the holder was positioned and balanced with the reference unit, then initial weights of the powders were recorded. The material was heated until 150 ^{o}C and waited 30 minutes to remove the moisture and then heated up to 1400 ^{o}C with a heating rate settled as 10 ^{o}C/min and the powders were oxidized. Afterwards, the ratio of weight changes (weight gains) to initial weights were calculated and converted to the percentages. Differential thermal analysis (DTA) was performed by thermocouples that were in contact with the sample holder and the reference unit [81].

2.8. Isoelectric Point (IEP) Measurements

Charge separation occurs as a result of suspensions of solid particles in liquid phase. This can happen either by ionization, ion adsorption or electronegativity differences of constituents. The resultant charge structure gives electrical double layer (EDL) [87]. In EDL, a layer is formed by oppositely charged ions associating the particle surface (Stern layer), while making another layer (Diffuse layer) in the liquid phase composed of mixed ions enriched with the rest of the oppositely charged ions. These two layers of ions in solution neutralize the surface charges. Zeta potential gives the potential on the shear plane which acts as a boundary for ions associate with the particle surface [88]. Isoelectric points of particles mean that the charges of the particles at their surfaces do not further affect the stabilization of the dispersion. This effect is an important parameter in stabilization of aqueous dispersions of colloidal particles [89].

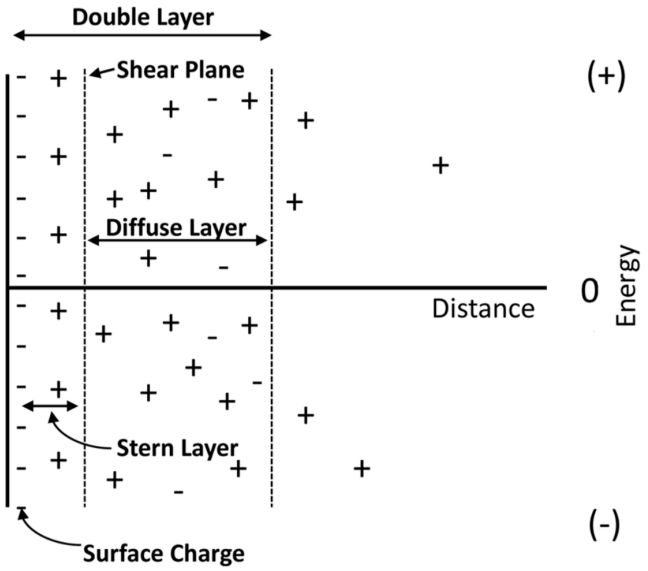

Figure 2.2. Schematic illustration of EDL model[88].

In this study, it was intended to change the surface acidity by reducing an oxide material which was TiO_2 (Rutile). Reduction was performed in Protherm tube furnace (ALSER, Ankara, Turkey). In such a procedure, the chemistry of the oxide material kept unaltered but the surface charges were influenced. Then, isoelectric point measurements were performed to analyze the change in surface charges of the reduced TiO_2 materials. Two methods were employed for zeta potential analyses. First, zeta potentials of oxide particles were measured manually in Dynamic Light Scattering (DLS) equipment (Zeta

sizer Nano ZS, Malvern Instruments Ltd., United Kingdom). Second, the experiments were performed with using an auto-titrator (MPT-2 Multi-Purpose Titrator, Malvern Instruments Ltd., United Kingdom).

For zeta potential study at Dynamic Light Scattering, first, suspensions were prepared by adding 5 mg of oxide powder to 100 ml of deionized water. The suspensions were dispersed in a sonicator (<10 mins). The pH values of suspensions were regulated by acidic and basic solutions (HCL & NH_3OH). The pH range for the measurements was between 2 and 4 since the zero zeta potential values were found to be in this range. Prepared solutions were taken by syringes and filled to the zeta potential cuvettes up to maximum filling level. Then, these cuvettes were placed inside the instrument and then were analyzed at least 3 times for a solution.

For zeta potential measurements with auto-titrator, another experimental procedure was followed. Buffer solutions were used to calibrate the pH values for the instrument (pH=4 & pH=9). Acidic and basic titrant solutions were prepared (0.5 M NaOH, 0.5 M HCl, 0.025 M HCl) and poured into their containers and positioned inside the MPT-2 auto-titrator. The titrant solutions were primed inside their tubes. Then, the suspensions were prepared by adding 5 mg of oxide powder to 100 ml of deionized water in a glassware. The suspensions were placed in a sonicator in order for particles to be well distributed in liquid (<10 mins). Then, at least 8ml of the liquid were taken and poured inside the titrator container and its magnetic stirrer was added. Zeta potential cuvette was attached to the plastic tube entrance and placed inside the Zeta sizer Nano ZS. Before starting the experiment, the zeta potential cuvette was filled with the mixture preventing the bubble formation inside.

Figure 2.3. Zeta Potential Instrument with Auto-titrator set-up.

2.9. Electrochemical Impedance Spectroscopy (EIS)

Impedance is defined as the ratio of voltage to current. However, it involves two terms named as real impedance and imaginary impedance. Real impedance is the resistance of the circuit to the flow of electric current. Imaginary impedance is related to the electrical energy stored in the circuit [90].

Electrochemical impedance spectroscopy can be performed in frequency range from kHz to mHz as in-situ measurement. The data is displayed either as Nyquist plots or Bode plots. The electrochemical processes can be studied by examining applied current change, temperature alterations, compositions of constituents. These parameters affect frequency shifts in the data so that the changes can be differentiated [91].

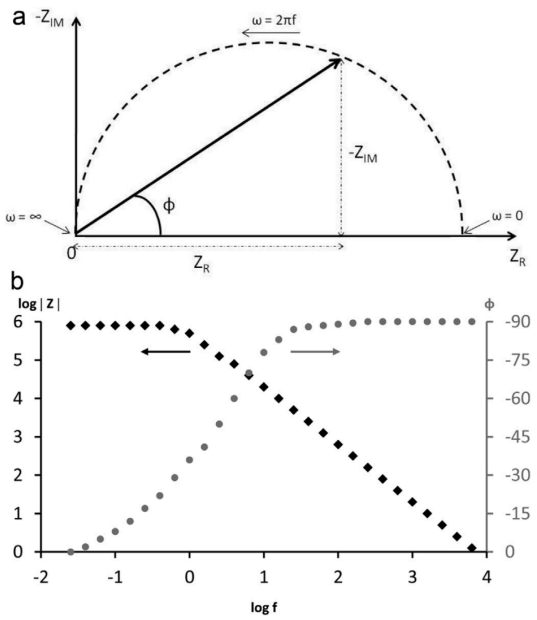

Figure 2.4. Graphical illustration of Nyquist and Bode plots as an example [91].

Another Nyquist plot with its low-amplitude harmonic current and corresponding cell voltage can be seen in figure below.

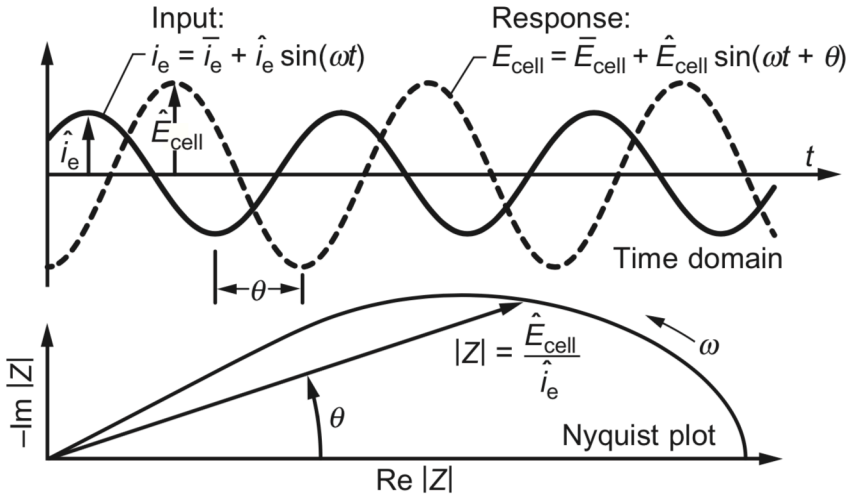

Figure 2.5. Parameters for electrochemical impedance spectroscopy [92].

The function of low-amplitude harmonic current depends on:

$$i_e(t) = \bar{\imath}_e + \hat{\imath}_e \sin(\omega t) \qquad \text{(Equation 2.1) [92]}$$

where ω is the frequency. Then, the cell voltage is also harmonic, with a shift in phase, due to the harmonic current and it depends on:

$$E_{cell}(t) = \bar{E}_{cell} + \hat{E}_{cell}\sin(\omega t + \theta) \quad \text{(Equation 2.2) [92]}$$

The phase shift θ and the ratio $\frac{\hat{E}_{cell}}{\hat{\imath}_e}$ depend on the frequency and the nominal operating current $\hat{\imath}_e$. By combining Euler's relation with voltage and current equations, the complex impedance Z depends on:

$$Z = \frac{\hat{E}_{cell}}{\hat{\imath}_e} e^{-j\theta} = \frac{\hat{E}_{cell}}{\hat{\imath}_e}(\cos\theta - j\sin\theta) \quad \text{(Equation 2.3) [92]}$$

where $j = \sqrt{-1}$.

Then, Z can be written in terms of its real and imaginary components:

$$Z = Z_R + jZ_{IM} \quad \text{(Equation 2.4) [90]}$$

There, Z_R and Z_{IM} stands for in-phase and out-of-phase part of the impedance.

For this research, before the measurements, the pellets that were pressed and sintered at 700 ^oC were applied flash-dry silver paste (SPI Supplies, West Chester, USA) to their top and bottom cross sectional surfaces acting as contact electrodes whereas pellet itself as electrolyte. The electrochemical impedance values of the ceramic composite electrolytes were examined by a two-probe AC impedance spectrometer (Solartron 1260, Farnborough, UK) and employing an electrochemical interface (Solartron 1286, Farnborough, UK) having an applied bias (AC) voltage amplitude of 100 mV. Frequency range of the measurements was from 1 Hz to 13 MHz. Temperature of the machine was settled to be heated up to 600 ^oC in order to perform the measurements from 600 ^oC to room temperature by attaching a ProboStatTM cell (NorECs, Oslo, Norway). The measurements were performed at air [16].

Then, the Nyquist plots were obtained and resistivity values with respect to temperature were analyzed. This was performed first by finding intercepts of the semicircles of the complex impedances plots with real axis. Analyses were done by using Z-view program (Scribner AI, Southern Pines, NC, USA). Then, the conductivity values were calculated. The following equations were used for resistivity (ρ) and conductivity (σ) calculations:

$$\rho = \frac{RA}{L} \quad \text{(Equation 2.5)}$$

$$\sigma = \frac{L}{RA} \quad \text{(Equation 2.6)}$$

Where R is the electrical resistance (ohm), L is the length of the material (m) and A is the cross-sectional area of the sample (m^2) i.e. area of the silver electrodes. Z view program was used to fit the high and low frequency data for RC equivalent circuit [93].

Figure 2.6. EIS setup in Sabancı University.

2.10. Brunauer-Emmett-Teller (BET) Surface Area Measurements

Brunauer-Emmett-Teller (BET) determined a way to analyze surface area of powders and porous materials depending mainly on nitrogen adsorption isotherms [94]. The theory behind BET analysis explains multilayer adsorption mechanism mathematically. It uses Langmuir isotherms [95] which is based on monolayers to extrapolate multilayers. In BET analysis it is assumed that the surfaces of adsorbents are completely flat so that the gas molecules can be adsorbed onto the surface or attached to the adsorbed gas molecules [96].

In BET analysis $(P/P_0)/\nu(1-P/P_0)$ is plotted as a function of P/P_0, where ν is the adsorption value at a certain relative pressure, P/P_0. A monolayer capacity, ν_m, is received by the slope, $c-1/\nu_m c$, and y intercept, $1/\nu_m c$, from a suitable linear region of the BET plot. The chosen pressure range values of $\nu(P_0-P)$ should be increasing with the relative pressure, P/P_0. The y intercept of the linear region must give a positive value to give a valid explanation for the c parameter (>0) [97]. The surface area is found as $A=\nu_m \sigma_0 N_{AV}$, where σ_0 is cross-sectional area of the gas (the ratio of the molar volume of the adsorbate gas to the mass of the solid sample or adsorbent) and N_{AV} is the Avogadro number [98].

BET surface area analyses were performed by BET 3 Flex instrument (Micromeritics, Norcross, USA).

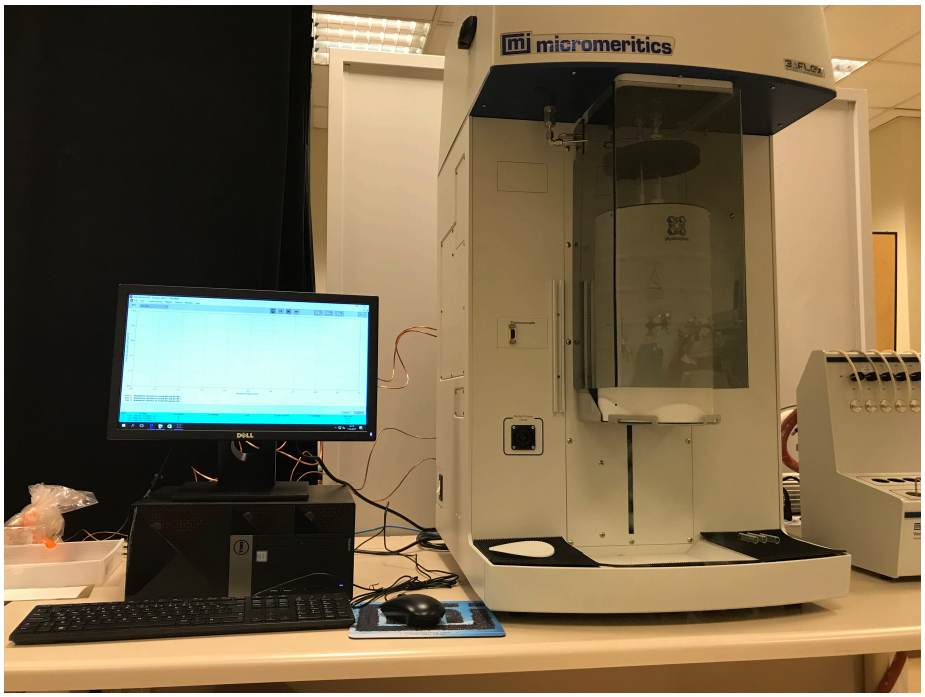

Figure 2.7. BET instrument in Sabancı University.

3. RESULTS

3.1. Composite Electrolyte

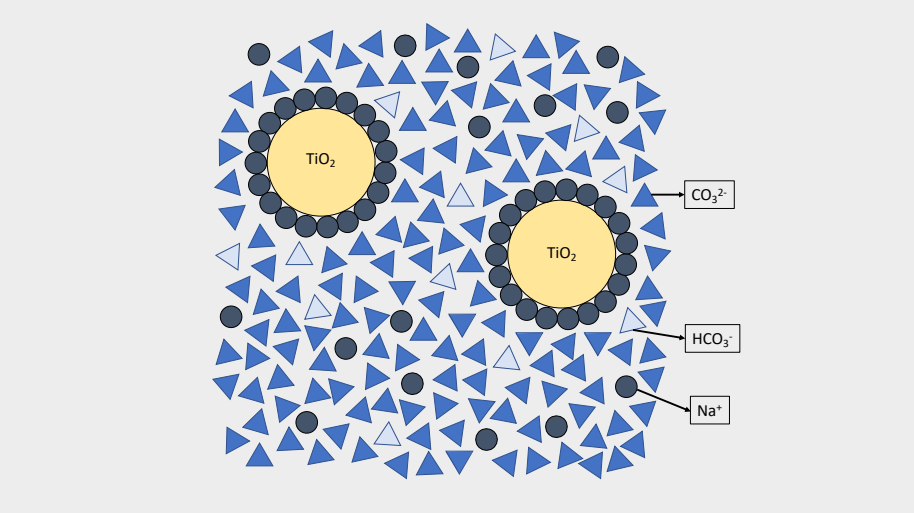

Figure 3.1. The composite electrolyte model.

The type and weight percentages of oxide and carbonate phases were the same for all pellets in order to see the effect of surface charge change. The amount of oxide phase was kept as 90 wt% and the amount of Na_2CO_3 phase was kept as 10 wt% of the total weight. The proposed schematic distribution of phases inside the composite electrolyte (pellet) can be seen in Figure 3.1.

Ionic conduction was facilitated in the regions in between oxide and carbonates in composite electrolytes. Oxide particles with a certain surface charge as determined by the isoelectric measurements attract oppositely charged counter-ions. The “co-ions” outside this region become free and move easier carrying the charges creating ionic conduction in electrolyte. These interactions of the oxide particles with the ions in the matrix of the electrolyte were schematically illustrated in Figure 3.1. These types of interactions were common in colloidal suspensions, soggy sand and solid nanocomposite electrolytes. These interactions also constitute the origin of electrical double layer concept and zeta potential analysis.

By reduction experiments, surface charges were altered intentionally creating defects in structure of TiO_2 (Rutile) powders and the corresponding changes were reported by

isoelectric point measurements, thermogravimetric analysis, XRD and SEM. Ionic conduction were measured by electrochemical impedance spectroscopy.

3.2. X-Ray Diffraction (XRD) Analysis Results

XRD analysis results of TiO_2 reduced at different temperatures were given in Figure 3.2. The intensity versus angle for the peak positions of TiO_2 powders were shown. As can be seen, XRD peak positions remained same for reduced TiO_2 powders. This means that there was not a phase change.

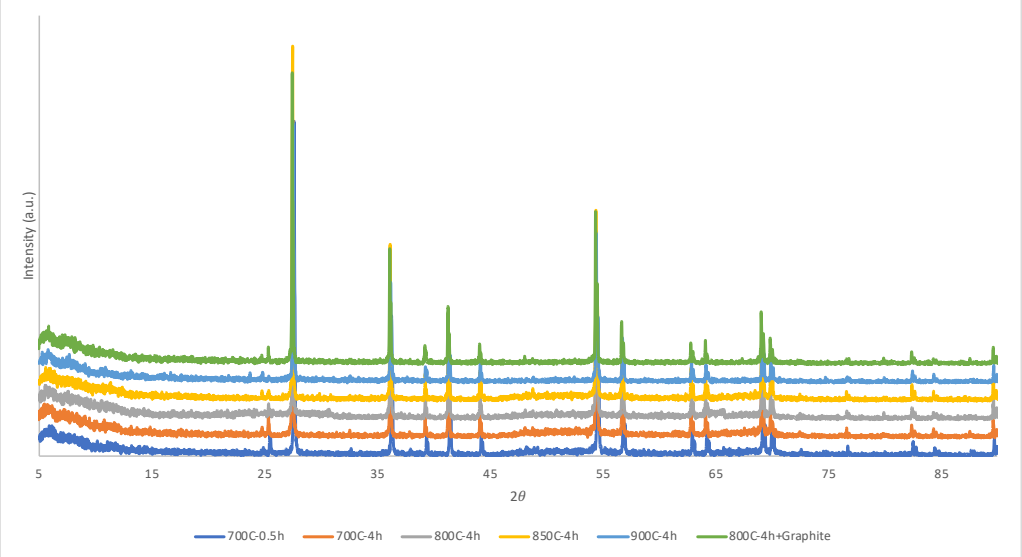

Figure 3.2. XRD analysis of reduced TiO_2 powders.

3.3. Thermogravimetric Analysis (TGA) Results

With the thermogravimetric analyses of TiO_2 powders that were reduced at temperatures of 700, 800, 850, 900, 1000 ^oC and for time intervals of 0.5 and 4 hours (see appendices), the weight changes were determined. The amount of weight that increased by temperature increase in TGA instrument was represented in Figure 3.3.

The resultant weight gain percentages of reduced TiO_2 powders were indicated in Figure 3.4. These weight changes obtained by thermal analyses corresponds to increase in weights because the reduced powders were fully re-oxidized in air atmosphere. Therefore, the amounts of weight gains were proportional to the reduction amount of powders which were treated under different processing conditions. The highest amount of reduction was

achieved for TiO_2 powder reduced at 800 ºC for 4 hours with graphite powders helping the reduction in the tube furnace. The amount of reduction was 6.71% which was observed as a weight gain after the oxidizing treatment in the TGA device. The figure indicates that with reduction temperature and time increasing, the amount of reduction also increased until 800 ºC. When the temperature was increased further beyond 800 ºC, the amount of reduction decreased.

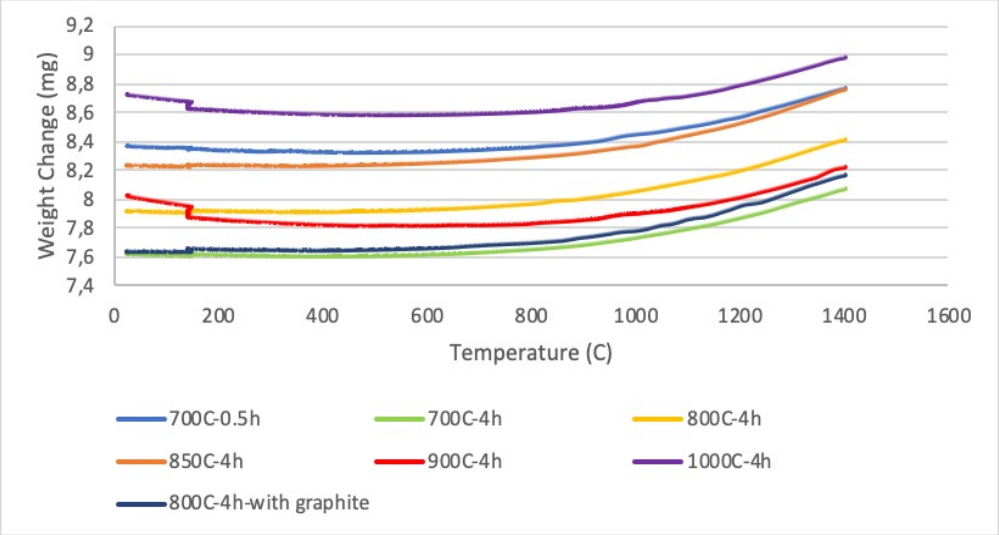

Figure 3.3. Increase in weight of TiO_2 powders that were heat treated in different temperatures and durations.

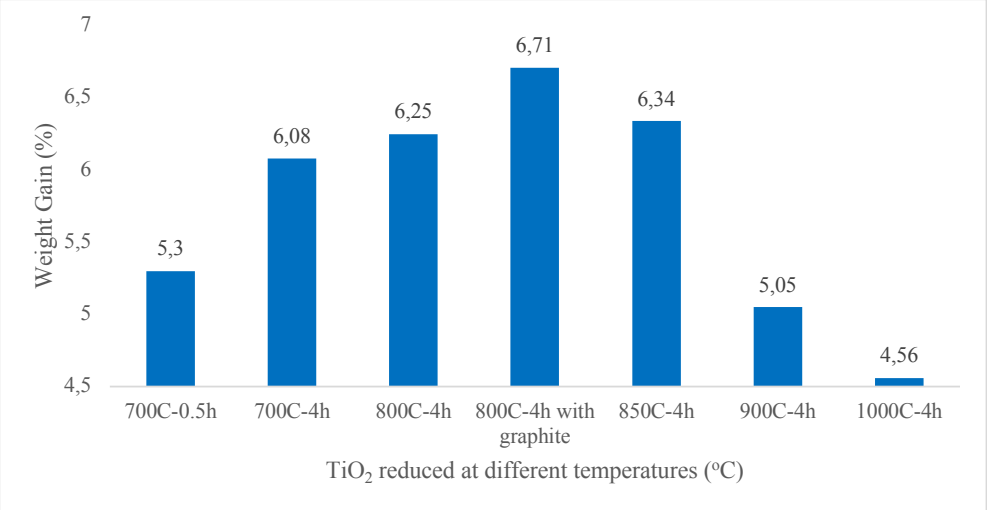

Figure 3.4. Weight gain percentages of reduced TiO_2 powders depending on processing temperatures and durations at tube furnace.

3.4. Isoelectric Point (IEP) Measurement Results

Isoelectric points of powders which were measured by auto-titration gave variable results (attached in appendices). In addition, depending on starting with acidic or basic pH values, the zeta potential curves changed. Therefore, manual measurements performed by DLS Zeta sizer Nano ZS instrument were considered for further evaluation.

Isoelectric points of as received and reduced TiO_2 powders which were measured as manually were represented in Figure 3.5. The higher the reduction temperatures, the smaller were the isoelectric point values of the TiO_2 powders until reduction temperature at 800 ^oC for 4 hours when graphite powder was also included in the environment. When the reduction temperatures increased beyond 800 ^oC, the isoelectric points of powders increased, this increase continued further until the powders that had reduction at 1000 ^oC for 4 hours.

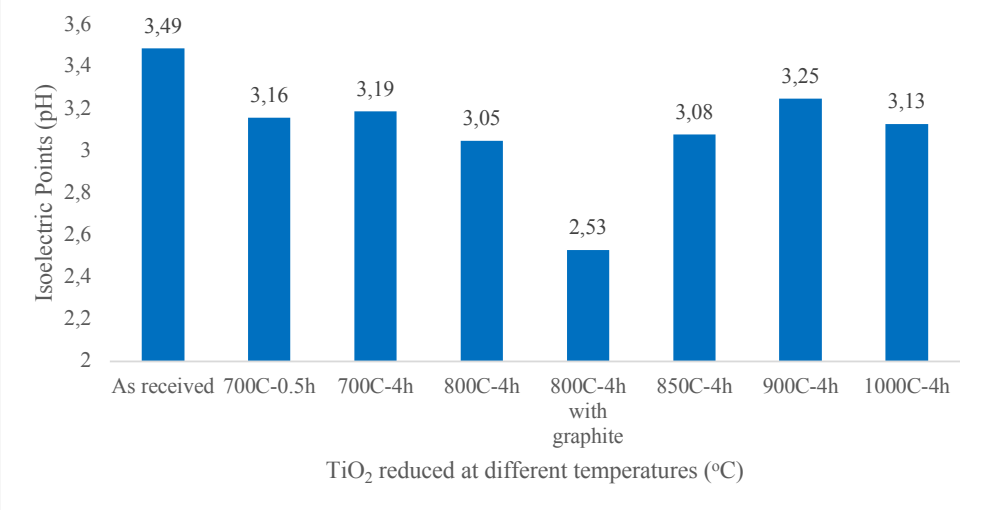

Figure 3.5. Isoelectric point change of reduced TiO_2 powders depending on processing temperatures and durations at tube furnace.

If the Figure 3.4 and 3.5 of thermal and isoelectric point analysis results considered together, it was understood that studied weight gains i.e. the former the reduction amounts of TiO_2 powders and their corresponding isoelectric points were interrelated and hence dependent on each other. Therefore, isoelectric points of these materials can be influenced by reduction amounts of rutile powders which were actually oxygen vacancies created in TiO_2 structure.

3.5. Scanning Electron Microscopy (SEM) Analysis Results

SEM analysis results of TiO_2 powders and nanocomposite pellets made up of TiO_2 and Na_2CO_3 powders can be found in the following figures.

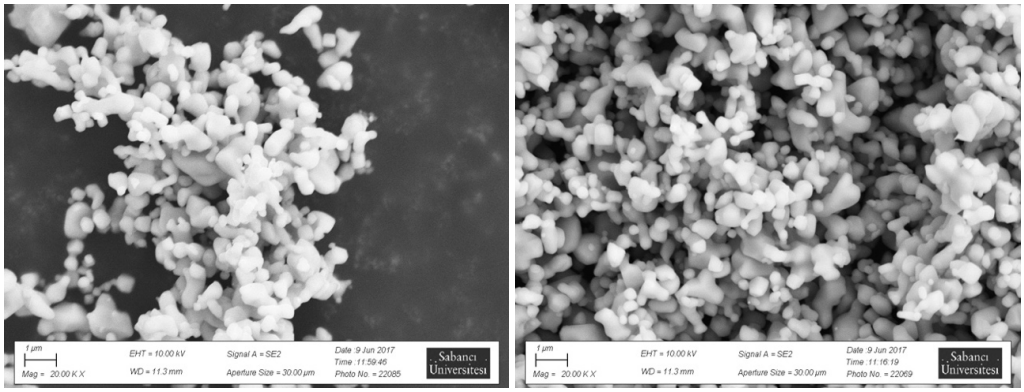

Figure 3.6. As received TiO_2 (Rutile) (left) and TiO_2 reduced at 700 °C for 4 hours (right).

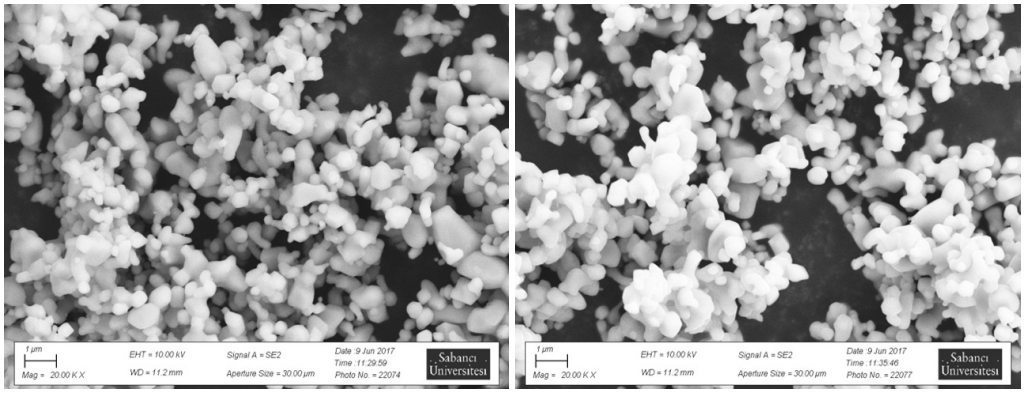

Figure 3.7. TiO_2 reduced at 800 °C for 4 hours (left) and at 850 °C for 4 hours (right).

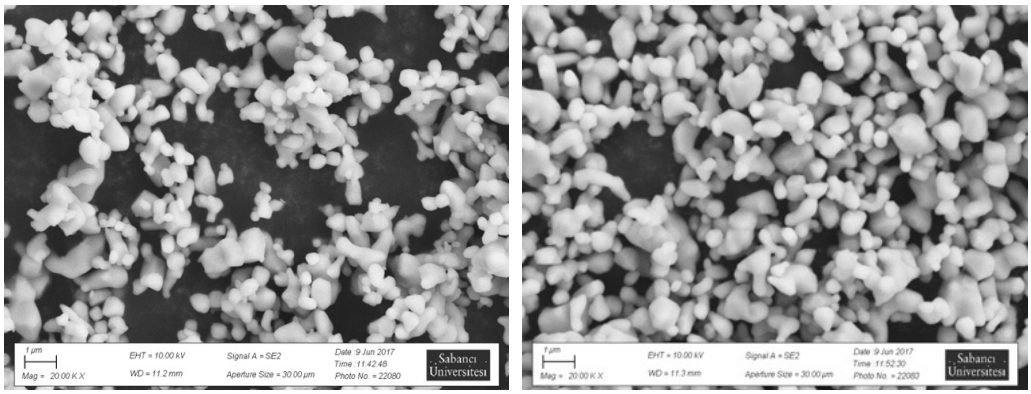

Figure 3.8. TiO_2 reduced at 900 °C for 4 hours (left) and at 1000 °C for 4 hours (right).

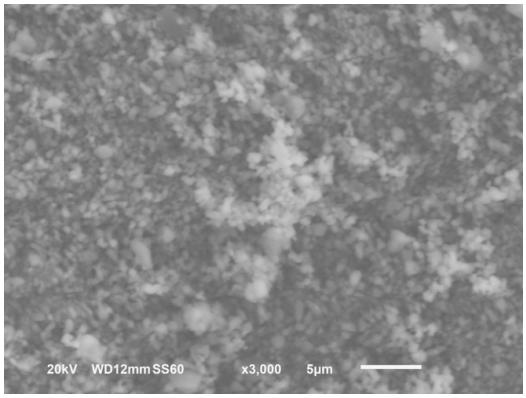

Figure 3.9. TiO_2 reduced at 700 °C for 30 minutes. Composite TiO_2-Na_2CO_3 10 wt%. Pellet heat treated at 700 °C for 1 hour.

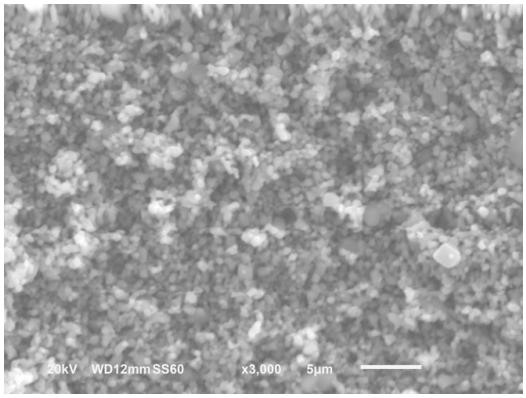

Figure 3.10. TiO_2 reduced at 700 °C for 4 hours. Composite TiO_2-Na_2CO_3 10 wt%. Pellet heat treated at 700 °C for 1 hour.

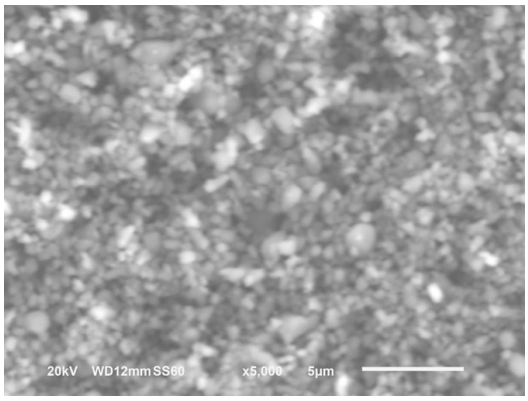

Figure 3.11. TiO_2 reduced at 800 °C for 4 hours. Composite TiO_2-Na_2CO_3 10 wt%. Pellet was heat treated at 700 °C for 1 hour.

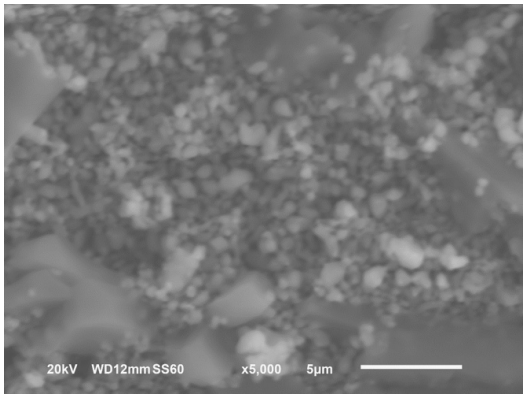

Figure 3.12. TiO_2 reduced at 850 °C for 4 hours. Composite TiO_2-Na_2CO_3 10 wt%. Pellet was heat treated at 700 °C for 1 hour.

3.6. Brunauer-Emmett-Teller (BET) Surface Area Measurement Results

BET surface area analysis of reduced TiO_2 powders performed at different dates can be seen in Table 3.1 and Table 3.2 below. The BET surface areas of these powders were variable although small surface area values were obtained for all samples. Yet, the trend was decrease in surface area when the reduction temperatures increases. Table 1 and Table 2 indicates the BET surface analysis results of reduced TiO_2 powders which were measured at different dates.

Table 3.1. BET surface analysis results of TiO_2 powder reduced at 700, 800 and 1000 ^oC for 4 hours in addition with graphite powders.

Sample Name	TiO_2 reduced at 700^oC for 4 hours with graphite	TiO_2 reduced at 800^oC for 4 hours with graphite	TiO_2 reduced at 1000^oC for 4 hours with graphite
BET Surface Area (m^2/g)	4.12	2.24	1.18

Table 3.2. BET surface analysis results of TiO_2 powder reduced at 800, 850 and 1000 ^oC for 4 hours in addition with graphite powders.

Sample Name	TiO_2 reduced at 800^oC for 4 hours with graphite	TiO_2 reduced at 850^oC for 4 hours with graphite	TiO_2 reduced at 1000^oC for 4 hours with graphite
BET Surface Area (m^2/g)	2.94	2.52	2.33

3.7. Electrochemical Impedance Spectroscopy (EIS) Results

Nyquist plots were obtained by electrochemical impedance analyses for all composite materials that were heated to 600 ºC and then cooled down step by step. At certain temperatures, the corresponding plots of imaginary and real impedance values were obtained. An example to these plots can be seen in Figure 3.13 and the rest can be found in appendix.

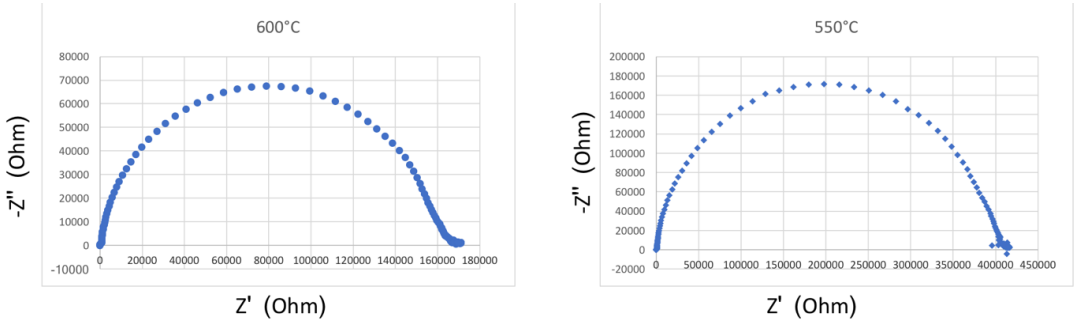

Figure 3.13. Impedance analyses of 10wt%Na_2CO_3-90wt%TiO_2 (reduced at 700 °C-4 hours) taken at 600 °C and 550 °C.

Reduction process affected the ionic conductivity of composite electrolytes. This effect can be studied by conductivity results of composite pellets obtained by electrochemical impedance spectroscopy method which were indicated in Figure 3.14. The curves show the change in the ionic conductivity of composites as a function of temperature. As the reduction temperature increased, reduction amounts increased and the curves shifted towards left. As the powders reduced more, the ionic conductivity decreased for composites prepared with TiO_2 powders reduced at specific temperatures as analyzed by EIS measurements.

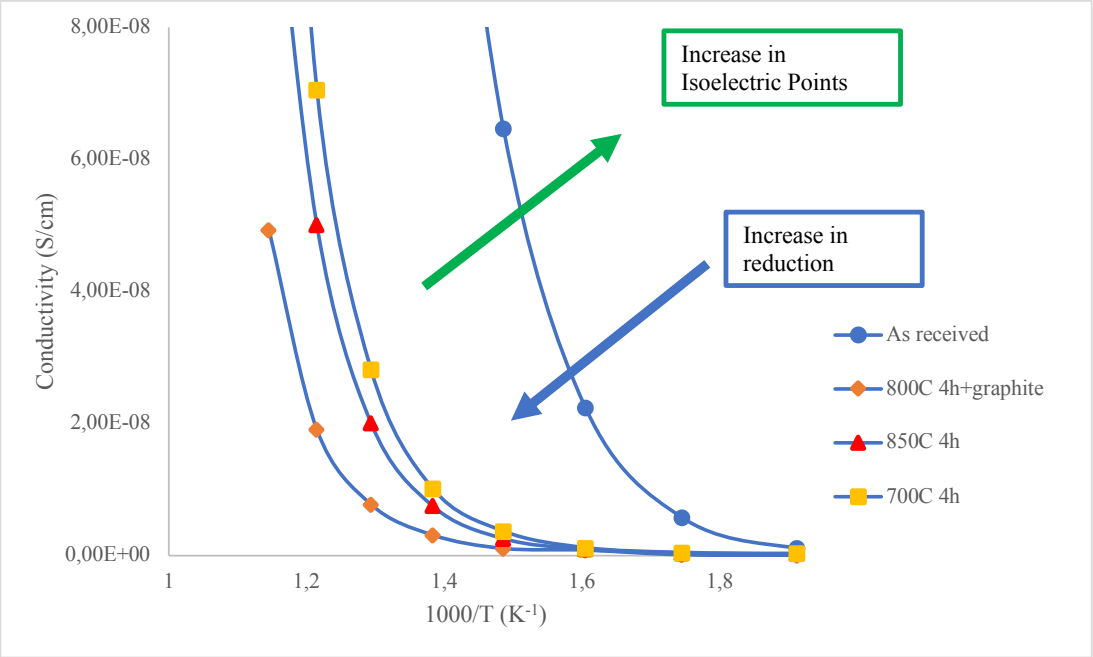

Figure 3.14. Conductivity (S/cm) vs 1000/Temperature (K^{-1}) for composite pellets composed of Na_2CO_3 and TiO_2 powders (as received and reduced at 800 (with graphite), 700, 850 °C for 4 hours).

The ionic conductivities of pellets obtained at certain temperatures in impedance measurements were indicated in Table 3.3, as a function of the reduction amount of TiO_2 powders. As it can be seen from the datasheet, conductivities of the nanocomposite pellets decreased as the reduction temperatures increased. The smallest ionic conductivity was measured in the composite prepared with TiO_2 powders reduced with the help of graphite powders which had the highest reduction amount as determined by the TGA.

Table 3.3. Ionic conductivity dependency of composite electrolytes, which involves different processes for TiO_2 reduction. Data obtained at certain temperatures of EIS.

Main Phase of Composite Electrolytes	Conductivity at 300 °C (S/cm)	Conductivity at 400 °C (S/cm)	Conductivity at 450 °C (S/cm)	Conductivity at 500 °C (S/cm)	Conductivity at 550 °C (S/cm)	Conductivity at 600 °C (S/cm)
Reduced TiO_2 (700 °C – 4 h)	4.97×10^{-10}	3.72×10^{-9}	1.02×10^{-8}	2.82×10^{-8}	7.06×10^{-8}	1.75×10^{-7}

Reduced TiO_2 (800 ^oC – 4 h)	$3.44x10^{-10}$	$2.88x10^{-9}$	$8.68x10^{-9}$	$1.18x10^{-8}$	$3.14x10^{-8}$	$6.59x10^{-8}$
Reduced TiO_2 (850 ^oC – 4 h)	$4.14x10^{-10}$	$2.57x10^{-9}$	$7.52x10^{-9}$	$2.01x10^{-8}$	$5.01x10^{-8}$	$1.12x10^{-7}$
Reduced TiO_2 (800 ^oC – 4 h + Graphite)	$1.41x10^{-10}$	$1.09x10^{-9}$	$3.13x10^{-9}$	$7.76x10^{-9}$	$1.91x10^{-8}$	$4.93x10^{-8}$

Figure 3.15a indicates the change in surface charges due to reduction treatments and their corresponding influence on percent weight gains. The figure is based on the TiO_2 powders treated at 800 ^oC with graphite, 800 ^oC, 850 ^oC and 700 ^oC for 4 hours. Reduction amount increased with increase in temperature of treatment. Including graphite also supported the increase in reduction amount. Increase in reduction amount of the powders modified the surface charges in other words it increased the surface acidity.

Ionic conductivity changes of reduced oxide materials measured at 450 ^oC and their isoelectric point dependency was indicated in Figure 3.15b. The conductivity values were based on the TiO_2 powders treated at 800 ^oC with graphite, 800 ^oC, 850 ^oC and 700 ^oC for 4 hours. This figure depicts that ionic conductivity of composites increased by increase in isoelectric points. Therefore, the less the reduction was, the more the ionic conductivity. Consequently, ionic conductivity increases with decrease in surface acidity.

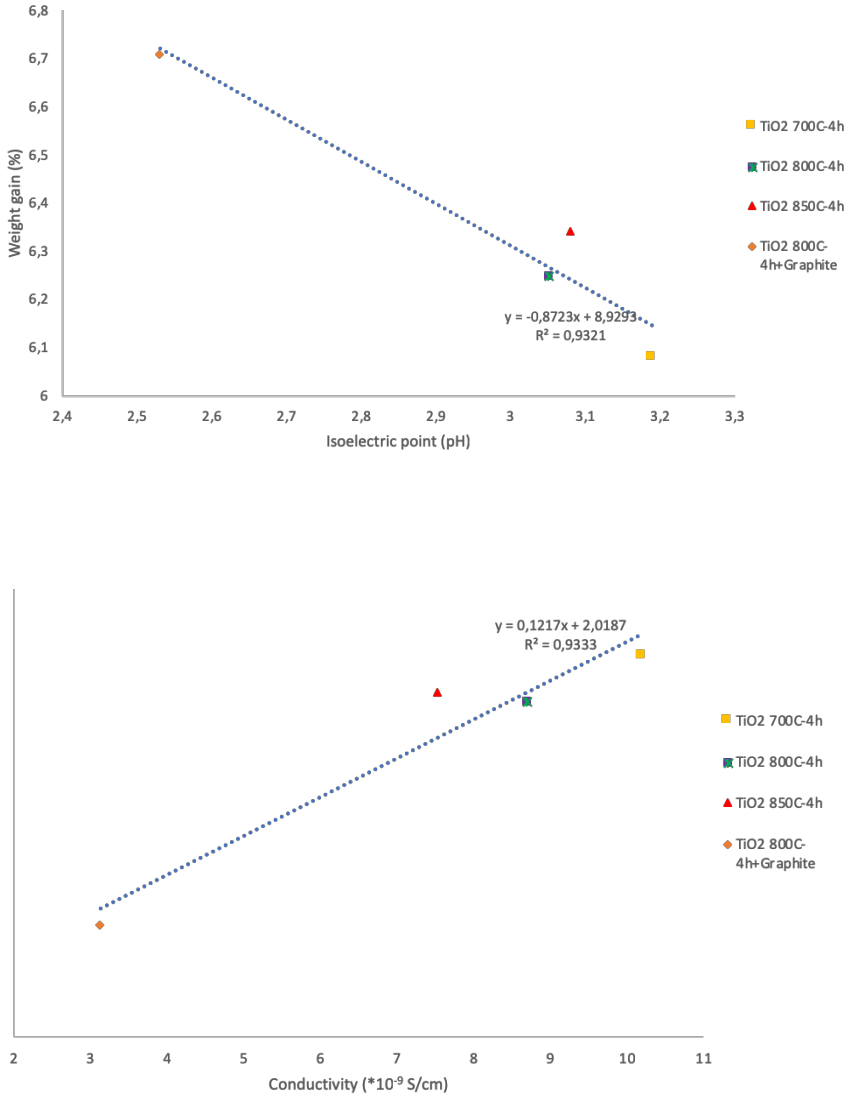

Figure 3.15. The correlation of Weight Gain (%) vs Isoelectric Point (pH) (3.15a) & Isoelectric Point (pH) vs Conductivity (S/cm) for the samples treated at 800 ºC – 4 h with graphite, 800 ºC – 4 h, 850 ºC – 4 h and 700 ºC – 4 h (3.15b) (values are taken for the case for 3.15b at 450ºC as an example).

As an example, for comparison, it is good to compare the data having two different process: for powder reduced at 800 ºC for 4 hours with graphite and at 700ºC for 4 hours. The former had a weight gain of 6.71 % which corresponds to an isoelectric point values of 2.53 and the ionic conductivity of the composite based on this powder was $3.13*10^{-9}$ S/cm. However, the weight gain of the latter was 6.08 % and the isoelectric point of it was 3.19 while the corresponding composite had an ionic conductivity value of $1.02*10^{-8}$ S/cm.

4. DISCUSSION

4.1. Defect Mechanism

Lattice defects are defects that disturb the atomic or ionic arrangement in a perfect crystal. These defects are important since they affect many characteristics such as electrical conductivity. Among all lattice defect types, point defects can be formed due to vacancy creation, interstitials, impurities and substitutional atoms [99].

In that respect, transition metal oxides can be successfully investigated regarding point defects. Transition metal oxides are the materials where the cations can easily alter the oxidation states. Therefore, the diffusion of ions depends mainly on oxygen partial pressure. The transition metal oxides in general can be either oxygen deficient or cation deficient materials. For example, TiO_2 used in this research is an oxygen deficient material and can be expressed as TiO_{2-x} [100].

This is because TiO_2 is among some ceramics which have tendency to be reduced easily thereby creating vacancies or deficiency of ions in its structure. The reduction of TiO_2 is a process where oxygen vacancies or Ti interstitials can be formed by heat treatments at reducing conditions. The defect formation has a notation which can be seen in equations 4.1 and 4.2 below [76]:

$$Ti_{Ti}{}^{x} + 2O_O{}^{x} \leftrightarrow Ti_i{}^{\cdots\cdot} + 4e' + O_2(g) \qquad \text{(Equation 4.1)}$$

$$Ti_{Ti}{}^{x} + 2O_O{}^{x} \leftrightarrow Ti_{Ti}{}^{x} + 2V_O{}^{\cdot\cdot} + O_2(g) + 4e' \qquad \text{(Equation 4.2)}$$

4.2. The Effect of Reduction on Defect Mechanism

Reduction heat treatment have a direct influence on defect mechanism. This influence is actually a weight loss resulted by oxygen vacancy formation in the structure of material thereby generating oxygen gas to the surroundings. Reduction of TiO_2 material was performed at different temperatures. To determine the amount of reduction achieved, thermogravimetric analysis was performed to oxidize the material under air flow. The amount and percentages of weight gain achieved in these oxide materials which were exposed to different treatment conditions can be seen in Figure 3.3 and 3.4.

The amount of weight gain increased with increasing reduction temperature until a reduction condition which was 800 ^{o}C for 4 hours with graphite addition. Beyond this temperature, the material behaved in a reverse way such that the weight gain percentages decreased with increasing temperature. The increase in weight gain percentage means that the material is actually reduced more. So, reduction amount first increased and after the specified temperature, it decreased. This behavior can be associated with particle size increase and coarsening happening in the TiO_2 at higher temperatures. After 800 ^{o}C, TiO_2 powders suffered from particle size growth which in turn affected the reduction amount. In other words, particle coarsening decreased the achieved reduction amount.

4.3. Reduction Treatment and the Influence on Particle Size Growth and the link with Ionic Conductivity

The earlier study of Shawuti and Gulgun proved the relationship between the ionic conductivity and particle size relation of composites, using different specific surface areas and impedance analyses. They showed that as the oxide particle sizes become smaller, with the increase in specific surface area, ionic conductivity values increased at all measurement temperatures. The interaction of the constituent phases directly affected the mobile ions at the interfaces. Thus, increasing the amount of interfaces between the oxide and carbonate (matrix) phases increased the ionic conduction. This is because interface regions between the oxide and matrix phases in composite electrolytes were shown to provide pathways for mobile ions [38].

Comparing the TiO_2 particles, it seemed that the size of the powders increased with increasing the reduction temperatures. Microstructural analyses supported this observation such that particles became appreciably larger.

Since particle size using Image J program could not be determined, it was decided to look at the percent change in particle sizes comparing the SEM pictures of TiO_2 reduced at 700 ^{o}C and 1000 ^{o}C. This was performed by choosing the particles having largest sizes in both pictures and evaluating the percent increase in size. The chosen particles in the regions marked as squares can be seen in figure 4.1 and 4.2.

For the TiO_2 particles reduced at 700 ^{o}C for 4 hours the total area (assuming a square size):

1*1.5 + 1.4*1.4 + 0.9*1.8 + 1.3*1.5 + 1.3*1.3 + 1.2*1 = 9.92 cm^2 (8.19 μm^2)

The total area of the marked square is: 12.1*12 = 145.2 cm^2 (120 μm^2)

(1 μm^2 corresponds to 1.21 cm^2 according to SEM picture.)

Ratio of the areas of particles to total area gives: 6.8%

For the TiO_2 particles reduced at 1000 ^oC for 4 hours the total area (assuming a square size):

1.8*1.5 + 0.9*1.8 + 1.8*1.2 + 1.5*1.4 + 1.9*1.5 + 2.1*1.6 = 14.79 cm^2 (12.22 μm^2)

The total area of the marked square is: 12.1*12 = 145.2 cm^2 (120 μm^2)

(1 μm^2 corresponds to 1.21 cm^2 according to SEM picture.)

Ratio of the areas of particles to total area gives: 10.2%

Based on the calculations, larger particles in TiO_2 reduced at 700 ^oC have 6.8% of the total area marked as square. However, the percentage of larger particles in TiO_2 reduced at 1000 ^oC was 10.2%. Therefore, there was an increase in the total area of larger particles as the reduction temperatures increased.

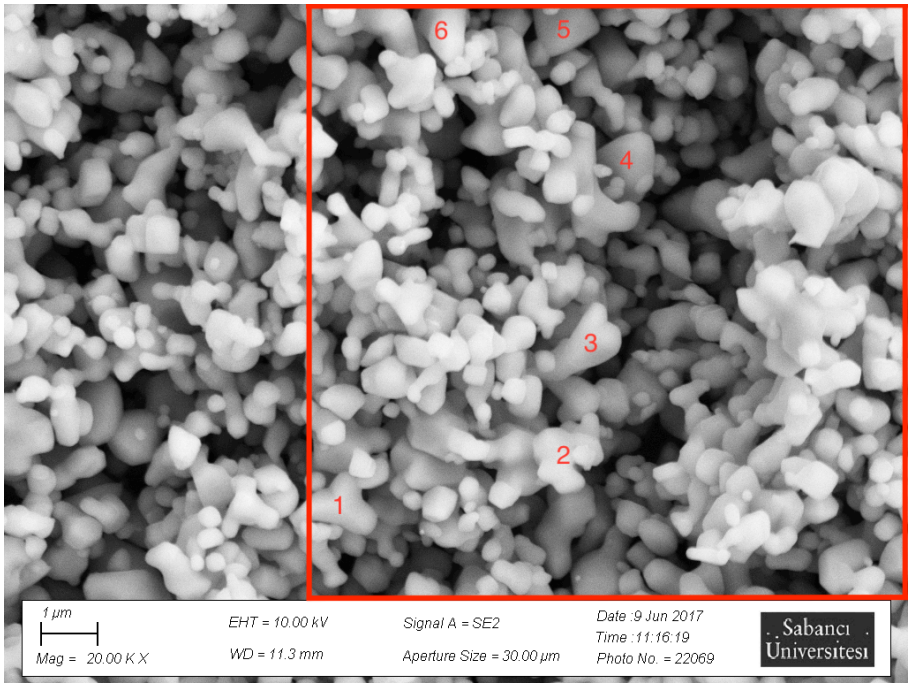

Figure 4.1. SEM picture of TiO_2 reduced at 700 °C for 4 hours.

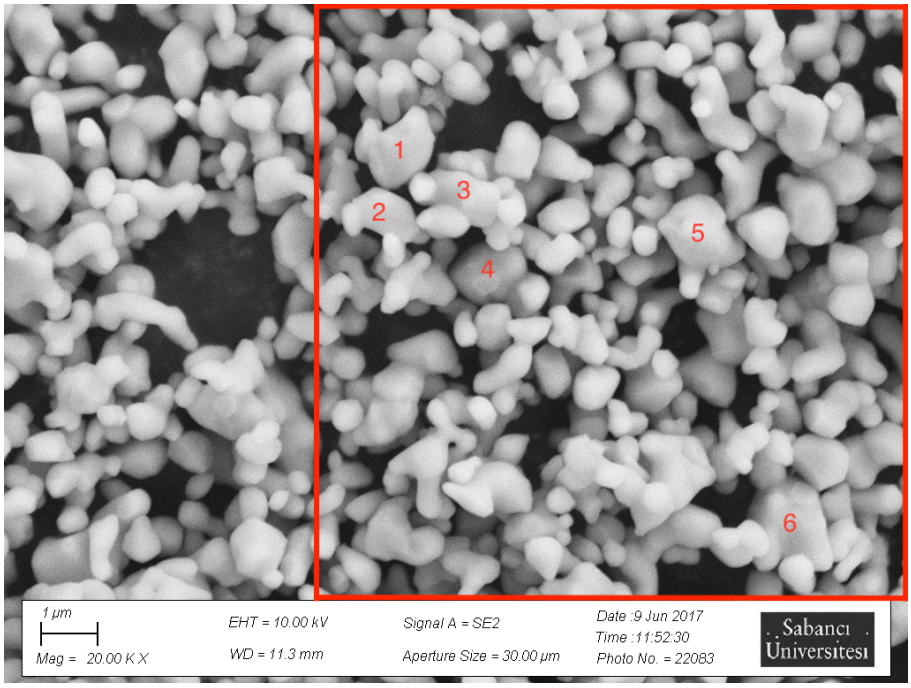

Figure 4.2. SEM picture of TiO_2 reduced at 1000 °C for 4 hours.

Particle size increase was also confirmed by BET surface area results. It was seen that as there was more reduction, the BET surface areas decreased. The decrease in surface area

means that particle sizes coarsen and as a result, ionic conduction pathways will be limited by the decrease in the number of interfaces. This is in correlation with particle size growth observed based on SEM images. Ionic conductivity results also supported the increase in the particle sizes such that there was a shift in their data towards the smaller ionic conductivity values according to the curves in figure 3.14. Thus, ionic conductivity of nanocomposite pellets decreased with an increase in reduction amount of TiO_2 powders and with the particle size growth. Particle coarsening causes a decrease in total interfacial area. Thus, there will not be as much available paths as before for ions to move through the interfacial regions. Therefore, mobility and diffusivity of ions at the interfaces are affected inversely.

4.4. Reduction Treatment and the Link between Surface Charges and Potential

The energy of a surface ion is affected by local atomic arrangements. Defect creation is ultimately linked with this situation. In other words, grain boundaries and their orientations, dislocations are important terms to determine the formation energies of defects [76]. Defects with different formation energies results in ion concentration gradient between bulk and the surfaces of grains. These differences create a charged region i.e. surface charge at the grain boundaries or surfaces. In order to balance the non-stoichiometry, a layer called space charge region is favorable and formed from the surface towards the center of the crystal with a distance (few to several hundred angstroms). So, the surface differs from the bulk in terms of electrostatic potential [76].

TiO_2 materials heat treated in reduced atmospheres leads to change in stoichiometry of the material. In as received case, the stoichiometry should be 1:2 in Ti:O ratio. With the reduction treatments the structure starts to give off its oxygen and results in oxygen deficiency which can be indicated as TiO_{2-x}. In addition, the color of TiO_2 can also change by reduction.

This is also because TiO_2 is a transition metal oxide that can easily become nonstoichiometric i.e. TiO_{2-x}. Ti^{4+} can be reduced to Ti^{3+} without destroying the structure. Oxygen vacancies are within the order of 1% which is the limit for stability of the oxide phase. Therefore, there will not be a phase change or decomposition into another phases [76]. However, defects that were created in oxide particles affected the surface charges of TiO_2 particles. The influence was both with the change in strength and sign of particles'

surface charges [76]. The point defects i.e. oxygen vacancies or Ti interstitials were created by reduction processes at variable temperatures which results in different surface charges for TiO_2 particles. When TiO_2 powders exposed to reduction, the defects formed in oxides let surface of particles to become more positive. This can be understood by positive potential at the interface which is given in figure 4.1. The positively charged surface is compensated by a negative space charge region inside the particle. Therefore, defects of negative effective charge (electrons) are concentrated in the vicinity of the region inside the boundary. On the other hand, depletion of positive effective charge defects (cation interstitials) is observed beneath the surface [76]. This mechanism can be followed in the figure 4.1.

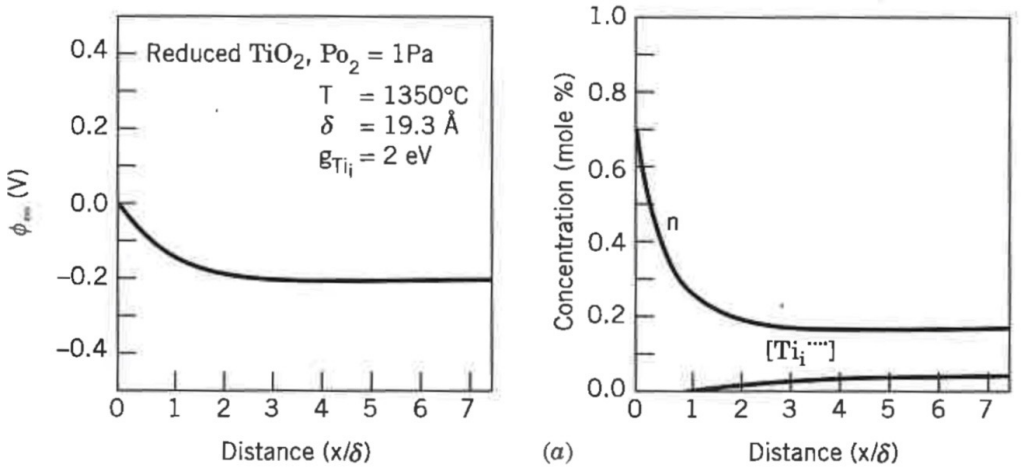

Figure 4.3. Space charge potential and spatial defect distribution for TiO_2, reprinted from [76] with permission.

Measurements performed with surface charges showed the interaction of reduction heat treatments with isoelectric points. The obtained information was such that isoelectric points decreased with increasing reduction amount which was measured by TGA analysis i.e. weight gains in oxidation. However, higher reduction temperatures (>800 ^oC) resulted in decrease in reduction amount i.e. less reduction. This was thought to be due to the effect of coarsening in nanoparticle sizes which in turn decreased the oxygen vacancy amounts at higher temperatures. This is because with the increase in particle sizes, the overall specific surface area of TiO_2 powders decreased. Then, there were not enough surfaces for ionic diffusion to take place and hence the defect concentrations at the interfaces decreased. Consequently, isoelectric points of TiO_2 particles were first

decreased with increase in reduction temperature but then they started to increase as further increase in reduction heat treatment temperatures.

There is an interaction between the amount of reduction and the surface charges of particles. This was understood by the weight gain increase and direct effect of decrease in isoelectric points of materials as clarified by obtained results. This interaction for IEP change can be expressed as (Weight Gain %)$^{2/3}$. Weight gain percentages are related to bulk oxygen vacancy concentration while the isoelectric points of particles are related with the ion concentrations at the surfaces. Therefore, it is necessary to express weight gain percentages in terms of surface ion concentrations. The ratio is proportional with the surface area and bulk volume: $\frac{Number\ of\ moles\ of\ ions\ in\ surface}{Number\ of\ moles\ of\ ions\ in\ bulk} = \frac{R^2}{R^3}$ assuming that particles have a spherical structure.

Weight percentages were also converted to atomic percentages for evaluation. When the reduction experiments performed, the total weight of TiO_2 powders were decreased by the amount of oxygen leaving the system. Therefore, weight actually decreased with a ratio: $\frac{O}{2O+Ti}$ = 16/80 = 1/5 or with an atomic ratio $\frac{O}{2O+Ti}$ = 1/3. So, the atomic percent was 5/3 of weight percent.

The percent atomic change and IEP proportion was close but not constant apart from the powders reduced with graphite environment. This can result from the size increase in TiO_2 particles which affected the surface areas. Therefore, surface area and volume ratio might not be constant. Also, the TiO_2 particles were not spherical but prismatic both in as received and reduced case. These particles also became agglomerated influencing the total surface area.

Table 4.1. Isoelectric point change based on as received TiO_2 and its relation with percent weight change at the surface of particles.

	700 °C - 0.5 h	700 °C - 4 h	800 °C - 4 h	800 °C - 4 h + Graphite	850 °C - 4 h	900 °C - 4 h	1000 °C - 4 h
IEP change with	0.33	0.3	0.44	0.96	0.41	0.24	0.36

respect to as received case							
Weight Gain %	0.053	0.0608	0.0625	0.0671	0.0634	0.0505	0.0456
Atomic %	0.088	0.101	0.104	0.112	0.106	0.084	0.076
(Atomic %)$^{2/3}$	0.198	0.217	0.221	0.232	0.224	0.192	0.179
Ratio of IEP to (Atomic %)$^{2/3}$	1.67	1.38	1.99	4.14	1.83	1.25	2.01

The higher the treatment temperature, the more the reduction occurred. Increase in reduction amount of the powders modified the surface charges in other words it increased the surface acidity. This means that isoelectric points of powders decreased by increase in the reduction amounts. Change in reduction amounts was understood by weight gains obtained by exposure to air atmosphere during TGA analyses. As there was more weight gain, isoelectric points decreased and vice versa.

4.5. Reduction Treatment and the Influence on Isoelectric Points and the link with Ionic Conductivity

There was a correlation with reduction amounts of TiO_2 powders, which affects isoelectric points, and ionic conductivities of nanocomposite electrolytes. Isoelectric points of powders decreased until the reduction at 800 ^oC, then with the particle size effect the isoelectric points increased back again with increasing the temperature of reduction treatments. Therefore, with the reduction amounts indicated by weight gains after re-oxidation, one can have an understanding about isoelectric points of materials which in turn affected the ionic conductivities. Ionic conductivity curves shifted to the lower values with the increase in reduction temperatures. This means that ionic conductivities and

isoelectric points are positively correlated to each other, if one increases the other increases as well.

Ionic conductivity is a product of mobility and free charge carriers. Since the mobility term is mainly affected by temperature change, number of free charge carriers are directly affecting ionic conductivity. Free charge carriers are proportional with isoelectric points and hence with weight gain percentages at the surfaces. The relation can be seen in Table 4.2. The values of coefficients were not matching. The difference could be due to the non-spherical TiO_2 particles and also atomic size and differences with O^{2-} ions that left the structures and CO_3^{2-} ions attaching to the surface of TiO_2 particles and their amounts. Therefore, the atomic size discrepancy could also be another reason for decrease in ionic conductivity.

Table 4.2. Ionic conductivity dependence of nanocomposites with corresponding weight gain percentages at the surfaces of TiO_2 particles.

	700 °C - 4 h	800 °C - 4 h	800 °C - 4 h + Graphite	850 °C - 4 h
Ionic conductivity of nanocomposite at 300 °C (S/cm)	4.97×10^{-10}	3.44×10^{-10}	1.41×10^{-10}	4.14×10^{-10}
Weight Gain %	0.0608	0.0625	0.0671	0.0634
Atomic %	0.101	0.104	0.112	0.106
$(\text{Atomic \%})^{2/3}$	0.217	0.221	0.232	0.224
Ratio of ionic conductivity to $(\text{Atomic \%})^{2/3}$	2.29×10^{-9}	1.56×10^{-9}	6.08×10^{-10}	1.85×10^{-9}

The number of surface attached ions influence the number of freed counter ions. Considering the reduction treatments of TiO_2 powders, the more the reduction we had,

the less the charge carriers it was obtained. Reduction heat treatments caused oxygen ion deficiencies in the TiO_2 particles. This affected the overall charge accumulation in the bulk itself. Oxygen ion deficiency at the boundaries was compensated by space charges inside. Therefore, further oxygen ion accumulation occurred towards the boundary. At the interfaces, due to the oxygen vacancies, remaining Ti^{4+} made a positively charged surface. Positively charged surface attracted negative counter ions (CO_3^{2-}) from the amorphous Na_2CO_3 matrix in nanocomposite pellets. This condition left less CO_3^{2-} charge carriers for ionic conduction there slowing down the ionic diffusion. Therefore, ionic conduction decreased.

5. CONCLUSION

There are basically two phenomena that affect the conductivity. Firstly, conductivity is affected by the change in reduction. Secondly, conductivity decreases due to the decrease in percolation and the decrease in the amount of the specific surface area or interface area. Hybrid fuel cells can show outstanding properties regarding ionic conduction. This is because conduction does not happen either in matrix or in solid oxide but in the interface between them. There is an interaction between the solid oxide and the amorphous salt matrix which resulted from surface charge. By using the same chemistry and performing the reduction experiments internal defect structure of the TiO_2 was changed. This affected the surface charges and the surface charges affected the ionic conductivity. By changing the oxygen content, surface charges could be influenced that could also affect the ionic conductivity. Therefore, the ionic conductivity of nanocomposites can be influenced by the isoelectric points and isoelectric points can be affected by changing the internal defect structure of the oxide particles. Therefore, the ionic conductivity of nanocomposites can be ultimately controlled by defect structure of the oxide material.

TiO_2 particles were exposed to reduction heat treatments under reducing atmospheres at different temperatures. During the research, thermogravimetric analyses performed to re-oxidize the reduced TiO_2 powders to see the percent gain in weight. Isoelectric point measurements were performed on as received and reduced TiO_2 materials to see the effect of reduction on surface acidity. Finally, nanocomposites were produced by as corresponding TiO_2 and Na_2CO_3 powders in defined compositions. Thermogravimetric analyses indicated that the highest percent value of gain in weight was 6.71% and isoelectric point measurements showed that the isoelectric point value of 2.53 was obtained for this reduced TiO_2 material giving the lowest value. This means that as reduction amount increases, isoelectric point decreases and surface acidity increases until particle size growth. As a result of this, ionic conductivity decreases.

REFERENCES

[1] A. Heinzel, M. Cappadonia, U. Stimming, K. V. Kordesch and J. C. T. Oliveira, "Fuel Cells," in *Ullmann's Encyclopedia of Industrial Chemistry*, Weinheim, Wiley-Vch, 2018.

[2] K. Othmer, "Fuel Cells," in *Encyclopedia of chemical technology*, vol. 12, New York, Wiley, 2005.

[3] S. M. Haile, "Fuel cell materials and components," *Acta Materialia,* vol. 51, p. 5981–6000, 2003.

[4] n. e. t. l. US department of energy office of fossil energy, "Fuel Cell handbook (Seventh ed.)," EG&G Technical service, Inc., 2016.

[5] D. J. Brett, A. Atkinson, N. P. Brandon and S. J. & Skinner, "Intermediate temperature solid oxide fuel cells," *Chemical Society Reviews,* vol. 37, no. 8, pp. 1568-1578, 2008.

[6] T. S. Lee, J. N. Chung and Y.-C. Chen, "Design and optimization of a combined fuel reforming and solid oxide fuel cell system with anode off-gas recycling," *Energy Convers Manage,* vol. 52, p. 3214–26, 2011.

[7] A. B. Stambouli and E. Traversa, "Solid oxide fuel cells (SOFCs): a review of an environmentally clean and efficient source of energy," *Renew Sustain Energy,* vol. 6, p. 433–55, 2002.

[8] S. Satyapal, Fuel Cell Technologies Overview, Washington, DC, 2012, pp. 1-46.

[9] N. Q. Minh, "Ceramic fuel cells," *Journal of the American Ceramic Society,* vol. 76, no. 3, pp. 563-588, 1993.

[10] B. Cook, "Introduction to fuel cells and hydrogen technology," *Engineering science and education journal,* vol. 11, no. 6, pp. 205-216, 2002.

[11] L. Carrette, K. A. Friedrich and U. & Stimming, "Fuel cells–fundamentals and applications," *Fuel Cells,* vol. 1, pp. 5-39, 2001.

[12] D. B. Stauffer, J. H. Hirschenhofer, M. G. Klett and R. R. & Engleman, Fuel Cell Handbook, Fourth Edition. doi:10.2172/14997., United States, 1998.

[13] W. Vielstich, H. A. Gasteiger and H. & Yokokawa, Handbook of Fuel Cells: Fundamentals Technology and Applications: Advances in Electrocatalysis, Materials, Diagnostics and Durability (Vol. 5), John Wiley & Sons, 2009.

[14] N. L. Rock, "Synthesis and characterization of novel electrocatalysts and supports for use in polymer electrolyte membrane fuel cells (Doctoral dissertation)," Carnegie Mellon University, 2009.

[15] R. J. Gorte, "Recent developments towards commercialization of solid oxide fuel cells," *AIChE journal,* vol. 51, no. 9, pp. 2377-2381, 2005.

[16] S. Shalima, "Ionic conduction mechanisms in nano-composite electrolyte and their relationship to micro-structural features (Doctoral dissertation)," Sabancı University, Istanbul, 2014.

[17] L. Yang, C. Zuo, S. Wang, C. Zhe and M. Liu, "A novel composite cathode for low temperature SOFCs based on oxide proton conductors," *Advanced Materials,* vol. 20, p. 3280–3283, 2008.

[18] L. Malavasi, C. A. J. Fisher and M. S. Islam, "Oxide-ion and proton conducting electrolyte materials for clean energy applications: structural and mechanistic features," *Chemical Society,* vol. 39, p. 4370–4387, 2010.

[19] W. Vielstich, A. Lamm and H. A. Gasteiger, "Handbook of Fuel Cells-Fundamentals," *Technology and Applications,* 2003.

[20] R. O. Fuentes and R. T. & Baker, "Synthesis and properties of Gadolinium-doped ceria solid solutions for IT-SOFC electrolytes," *International Journal of Hydrogen Energy,* vol. 33, no. 13, pp. 3480-3484, 2008.

[21] L. Carrette, K. A. Friedrich and U. Stimming, "Fuel cells: principles, types, fuels, and applications," *ChemPhysChem,* vol. 1, p. 162–193, 2000.

[22] S. Sanna, V. Esposito, D. Pergolesi, A. Orsini, A. Tebano, S. Licoccia, G. Balestrino and E. Traversa, "Fabrication and electrochemical properties of epitaxial samarium- doped ceria films on SrTiO3-buffered MgO substrates," *Advanced Functional Materials,* vol. 19, pp. 1713-1719, 2009.

[23] H. Nomura, S. Parekh, J. Selman and S. J. Al-Hallaj, "Fabrication of YSZ electrolyte for intermediate temperature solid oxide fuel cellusing electrostatic spray deposition: II–cell performance," *Applied Electrochemistry,* vol. 35, p. 1121–1126, 2005.

[24] Z. Naiqing, S. Kening, Z. Derui and D. J, "Study on properties of LSGM electrolyte made by tape casting method and applications in SOFC," *Journal of Rare Earths,* vol. 24, pp. 90-92, 2006.

[25] B. Zhu, "Functional ceria–salt-composite materials for advanced ITSOFC applications.," *Journal Power Sources,* vol. 114, p. 1–9, 2003.

[26] B. Zhu and M. D. Mat, "Studies on dual phase ceria-based composites in electrochemistry.," *International Journal of Electrochemical Science,* vol. 1, p. 383–402, 2006.

[27] X. Wang, Y. Ma, R. Raza, M. Muhammed and B. Zhu, "Novel core–shell SDC/amorphous Na2CO3 nanocomposite electrolyte for low-temperature SOFCs.," *Electrochemistry Communications,* vol. 10, p. 1617–1620, 2008.

[28] F. Tietz, H. P. Buchkremer and D. Stöver, *Solid State Ionics,* 2002.

[29] M. M. Mench, *Mech. Eng. Handb. Energy Power Third Ed.,* 2006.

[30] M. G. Bellino, D. G. Lamas and d. R. N. E. Walsöe, "Enhanced ionic conductivity in nanostructured, heavily doped ceria ceramics," *Advanced Functional Materials,* vol. 16, p. 107–113, 2006.

[31] R. Raza, X. Wang, Y. Ma, X. Liua and B. Zhu, "Improved ceria–carbonate composite electrolytes.," *International Journal of Hydrogen Energy,* vol. 35, p. 2684–2688, 2010.

[32] B. Zhu, "Solid oxide fuel cell (SOFC) technical challenges and solutions from nano-aspects.," *International Journal of Energy Research,* vol. 33, no. 13, pp. 1126-1137, 2009.

[33] A. Tschöpe, "Grain size-dependent electrical conductivity of polycrystalline cerium oxide II: Space charge model Author links open overlay panel," *Solid State Ionics,* vol. 39, no. 3–4, pp. 267-280, 2001.

[34] J. Maier, *Nature Materials,* vol. 4, p. 805, 2005.

[35] J. Jamnik, J. Maier and S. Pejovnik, *Solid State Ionics,* p. 75:51, 1995.

[36] J. Lee, S. Adams and J. Maier, "Lee J, Adams S, Maier J.," *Journal of the Electrochemical Society,* vol. 147, p. 2407, 2000.

[37] Y. Ma, X. D. Wang, M. Muhammed and B. Zhu, "Thermal stability study of SDC/NaCO3 nanocomposite electrolyte for low-temperature SOFCs.," *International Journal of Hydrogen Energy, in press.*.

[38] S. Shawuti and M. A. & Gülgün, "Solid oxide-molten carbonate nano-composite fuel cells: Particle size effect. doi:10.1016/j.jpowsour.2014.05.010," *Journal of Power Sources,* vol. 267, pp. 128-135, 2014.

[39] L. Qinghua and B. Zhu, *Appl Phys Lett,* vol. 97, p. 183115, 2010.

[40] M. G. Bellino, D. G. Lamas and N. E. Walsöe de Reca, *J Mater Chem,* vol. 18, p. 4537, 2008.

[41] B. Zhu, "Functional ceria–salt-composite materials for advanced ITSOFC applications. doi:10.1016/s0378-7753(02)00592-x," *Journal of Power Sources,* vol. 114, no. 1, pp. 1-9, 2003.

[42] B. Zhu, "Advantages of intermediate temperature solid oxide fuel cells for tractionary applications. doi:10.1016/s0378-7753(00)00564-4," *Journal of Power Sources ,* vol. 93, no. 1-2, pp. 82-86, 2001.

[43] W. Zhu, C. Xia, D. Ding, X. Shi and G. & Meng, "Electrical properties of ceria-carbonate composite electrolytes. doi:10.1016/j.materresbull.2006.04.001," *Materials Research Bulletin,* vol. 41, no. 11, pp. 2057-2064, 2006.

[44] X. Li, G. Xiao and K. & Huang, "Effective ionic conductivity of a novel intermediate-temperature mixed oxide-ion and carbonate-ion conductor," *Journal of The Electrochemical Society,* vol. 158, no. 2, pp. 225-232, 2011.

[45] B. Zhu, "Proton and oxygen ion-mixed-conducting ceramic composites and fuel cells. doi:10.1016/s0167-2738(01)00933-x," *Solid State Ionics,* vol. 145, no. 1-4, pp. 371-380, 2001.

[46] G. Abbas, R. Raza, M. A. Chaudhry and B. & Zhu, "Preparation and characterization of nanocomposite calcium doped ceria electrolyte with alkali carbonates (NK-CDC) for SOFC," *Journal of Fuel Cell Science and Technology,* vol. 8, no. 4, p. 041013, 2011.

[47] B. Zhu, S. Li and B. E. Mellander, *Electrochemistry Communications,* vol. 10, p. 302, 2008.

[48] S. Shawuti and M. A. & Gülgün, "Solid oxide carbonate composite fuel cells: Size effect on percolation," *International Journal of Hydrogen Energy,* vol. 41, no. 44, pp. 20343-20349, 2016.

[49] X. Wang, "Ionic Conducting Composite as Electrolyte for Low Temperature Solid Oxide Fuel Cells (Doctoral dissertation, Royal institute of technology).," 2010.

[50] A. J. Bhattacharyya, J. Fleig, Y.-G. Guo and J. Maier, *Adv. Mater.,* vol. 17, p. 2630, 2005.

[51] S. K. Das and A. J. & Bhattacharyya, "Oxide Particle Surface Chemistry and Ion Transport in “Soggy Sand” Electrolytes. doi:10.1021/jp810761e," *The Journal of Physical Chemistry C,* vol. 113, no. 16, pp. 6699-6705, 2009.

[52] C. Pfaffenhuber, M. Göbel, J. Popovic and J. & Maier, "Soggy-sand electrolytes: status and perspectives," *Physical Chemistry Chemical Physics,* vol. 15, no. 42, pp. 18318-18335, 2013.

[53] A. M. Stephan and K. S. & Nahm, "Review on composite polymer electrolytes for lithium batteries," *Polymer,* vol. 47, no. 16, pp. 5952-5964, 2006.

[54] J. Maier, "Ionic conduction in space charge regions," *Progress in solid state chemistry,* vol. 23, no. 3, pp. 171-263, 1995.

[55] C. C. Liang, "Conduction characteristics of the lithium iodide-aluminum oxide solid electrolytes," *Journal of the Electrochemical Society,* vol. 120, no. 10, pp. 1289-1292, 1973.

[56] A. K. Shukla, N. Vaidehi and K. T. & Jacob, "Ionic conduction in dispersed solid-electrolytes," *Journal of Chemical Sciences,* vol. 96, no. 6, pp. 533-547, 1986.

[57] J. B. Wagner, "Composite solid ion conductors (T. Takahashi, Ed.)," in *High conductivity solid ionic conducters*, Singapore, World scientific, 1989.

[58] J. Maier, "Enhancement of the Ionic Conductivity in Solid-Solid-Dispersions by Surface Induced Defects. doi:10.1002/bbpc.198400007," *Berichte Der Bunsengesellschaft Für Physikalische Chemie,* vol. 88, no. 11, pp. 1057-1062, 1984.

[59] J. Maier, "Surface Induced Defects in the Space Charge Region and the Enhancement of Ionic Conductivity in Two-Phase Systems," *Physica status solidi (b),* vol. 123, no. 1, pp. 89-91. , 1984.

[60] J. Maier, "Kröger-vink diagrams for boundary regions. doi:10.1016/0167-2738(89)90351-2," *Solid State Ionics,* Vols. 32-33, pp. 727-733, 1989.

[61] J. Maier, "Ionic conduction in space charge regions," *Progress in solid state chemistry,* vol. 23, no. 3, pp. 171-263, 1995.

[62] J. Maier, "Defect chemistry and conductivity effects in heterogeneous solid electrolytes," *Journal of the Electrochemical Society,* vol. 134, no. 6, pp. 1524-1535 , 1987.

[63] Y. Saito and J. & Maier, "Ionic conductivity enhancement of the fluoride conductor CaF2 by grain boundary activation using Lewis acids," *Journal of the Electrochemical Society,* vol. 142, no. 9, pp. 3078-3083, 1995.

[64] T. Jow and J. B. & Wagner, "The effect of dispersed alumina particles on the electrical conductivity of cuprous chloride," *Journal of the Electrochemical Society,* vol. 126, no. 11, pp. 1963-197, 1979.

[65] N. Vaidehi, R. Akila, A. K. Shukla and K. T. & Jacob, "Enhanced ionic conduction in dispersed solid electrolyte systems CaF2-Al2O3 and CaF2-CeO2," *Materials research bulletin,* vol. 21, no. 8, pp. 909-916, 1986.

[66] A. K. Shukla, R. Manoharan and J. B. & Goodenough, "Enhancement of ionic conductivity by dispersed oxide inclusions: Influence of oxide isoelectric point and cation size," *Solid State Ionics,* vol. 26, no. 1, pp. 5-10, 1988.

[67] K. Hariharan and J. & Maier, "Enhancement of the Fluoride Vacancy Conduction in PbF2: SiO2 and PbF2: Al2 O3 Composites.," *Journal of the Electrochemical Society,* vol. 42, no. 10, pp. 3469-3473 , 1995.

[68] Y. Liu, B. Li, X. Wei and W. Pan, "Citric–Nitrate Combustion Synthesis and Electrical Conductivity of the Sm3+ and Nd3+ Co-Doped Ceria Electrolyte.," *American Chemical Society,* 2008.

[69] R. B. Schoch, J. Han and P. Renaud, "Transport phenomena in nanofluidics.," *Reviews of Modern Physics,* vol. 80, p. 839, 2008.

[70] J. T. G. Overbeek, "Colloid Science (H. R. Kruyt, ed.)," *Elsevier,* vol. I, 1952.

[71] G. Wang, W. Brown and M. Kvetny, "Structure and dynamics of nanoscale electrical double layer," *Elsevier,* vol. 13, pp. 112-118, 2019.

[72] "Stabilizing titanium dioxide," European Coatings Journal.

[73] G. A. Parks, "The Isoelectric Points of Solid Oxides, Solid Hydroxides, and Aqueous Hydroxo Complex Systems," *Chemical Reviews,* vol. 65, no. 2, p. 177–198, 1965.

[74] I. S. Bouhaik, P. Leroy, P. Ollivier, M. Azaroual and L. & Mercury, "Influence of surface conductivity on the apparent zeta potential of TiO2 nanoparticles: Application to the modeling of their aggregation kinetics. doi:10.1016/j.jcis.2013.05.034," *Journal of Colloid and Interface Science,* vol. 406, pp. 75-85, 2013.

[75] J. Maier, 1995.

[76] Y. Chiang, D. P. Birnie and W. D. & Kingery, Physical ceramics: principles for ceramic science and engineering, New York: Wiley, 1997.

[77] B. Zhu, "Next generation fuel cell R&D," *International Journal of Energy Research,* vol. 30, p. 895–903, 2006.

[78] A. Bouzoubaa, A. Markovits, M. Calatayud and C. & Minot, "Comparison of the reduction of metal oxide surfaces: TiO2-anatase, TiO2-rutile and SnO2-rutile. doi:10.1016/j.susc.2005.03.029," *Surface Science,* vol. 583, no. 1, pp. 107-117, 2005.

[79] M. Menetrey, A. Markovits, C. Minot and G. Pacchioni, *J. Phys. Chem. B,* vol. 108, p. 12858, 2004.

[80] G. Gregori, R. Merkle and J. & Maier, "Ion conduction and redistribution at grain boundaries in oxide systems. doi:10.1016/j.pmatsci.2017.04.009," *Progress in Materials Science,* vol. 89, pp. 252-305, 2017.

[81] J. S. Reed, Principles of ceramic processing, New York: Wiley, 1995.

[82] T. P. Yadav, R. M. Yadav and D. P. & Singh, "Mechanical milling: a top down approach for the synthesis of nanomaterials and nanocomposites. Nanoscience and Nanotechnology," vol. 2, no. 3, pp. 22-48, 2012.

[83] P. Khadka, J. Ro, H. Kim, I. Kim, J. T. Kim, H. Kim, ... and J. & Lee, "Pharmaceutical particle technologies: An approach to improve drug solubility, dissolution and bioavailability.," *Asian journal of pharmaceutical sciences,* vol. 9, no. 6, pp. 304-316, 2014.

[84] K. D. Vernon-Parry, "Scanning electron microscopy: an introduction.," *III-Vs Review,* vol. 13, no. 4, pp. 40-44, 2000.

[85] C. Giannini, M. Ladisa, D. Altamura, D. Siliqi, T. Sibillano and L. & De Caro, "X-ray diffraction: a powerful technique for the multiple-length-scale structural analysis of nanomaterials.," *Crystals,* vol. 6, no. 8, p. 87, 2016.

[86] M. Wagner, Thermogravimetric Analysis. In Thermal analysis in practice, München: Hanser, 2017.

[87] A. I. Gómez-Merino, F. J. Rubio-Hernández, J. F. Velázquez-Navarro and J. & Aguiar, "Estimation of ion diffusion coefficients at the stagnant layer using TiO2 aqueous suspension zeta potential data.," *Soft Materials,* vol. 13, no. 3, pp. 127-137, 2015.

[88] J. J. Carlson and S. K. & Kawatra, "Factors affecting zeta potential of iron oxides.," *Mineral Processing and Extractive Metallurgy Review,* vol. 34, no. 5, pp. 269-303, 2013.

[89] G. G. Liang, B. S. Hawkett and R. I. & Tanner, "The determination of the isoelectric point from measurements of dispersion viscosity as a function of pH," *Journal of dispersion science and technology,* vol. 26, no. 4, pp. 469-472, 2005.

[90] V. F. Lvovich, Impedance Spectroscopy: Applications to Electrochemical and Dielectric Phenomena, New Jersey: J. Wiley & Sons, Hoboken, 2008.

[91] A. Nechache, M. Cassir and A. & Ringuedé, "Solid oxide electrolysis cell analysis by means of electrochemical impedance spectroscopy: A review.," *Journal of Power Sources,* vol. 258, pp. 164-181, 2014.

[92] R. J. Kee, H. Zhu, R. J. Braun and T. L. & Vincent, "Modeling the steady-state and dynamic characteristics of solid-oxide fuel cells," *Advances in Chemical Engineering,* vol. 41, pp. 331-381, 2012.

[93] E. Barsoukov and J. R. Macdonald, New Jersey: John Wiley & Sons 2nd Edition, 2005.

[94] F. Rouquerol, J. Rouquerol and K. S. W. Sing, Adsorption by Powders and Porous Solids; Principles, Methodology and Applications, San Diego, CA, 1999.: Academic Press, 1999.

[95] I. Langmuir, *J. Am. Chem. Soc. ,* vol. 38, p. 2221, 1916.

[96] T. S. Van Erp and J. A. Martens, "A standardization for BET fitting of adsorption isotherms," *Microporous and Mesoporous Materials,* vol. 145, no. 1-3, pp. 188-193, 2011.

[97] J. Rouquerol, P. Llewellyn and F. Rouquerol, *Stud. Surf. Sci. Catal.,* vol. 160, p. 49, 2007.

[98] K. C. Kim, T. U. Yoon and Y. S. & Bae, "Applicability of using CO2 adsorption isotherms to determine BET surface areas of microporous materials," *Microporous and Mesoporous Materials,* vol. 224, pp. 294-301, 2016.

[99] H. Yanagida, K. Koumoto and M. & Miyayama, The chemistry of ceramics, Chichester: Wiley, 1996.

[100] R. Riedel and I. (. Chen, Ceramics science and technology, Weinheim: Willey-Vch, 2008.

APPENDICIES

Appendix 1:

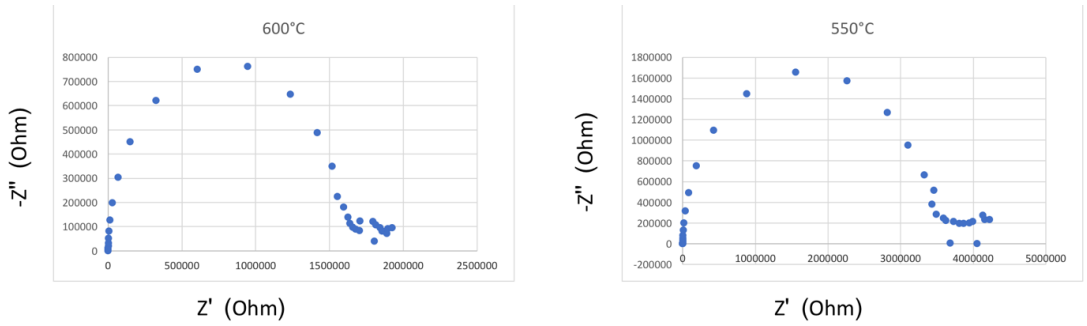

Figure: Impedance analyses of 10%Na_2CO_3-90%TiO_2 (reduced at 700°C-0.5 hours) taken at 600°C and 550°C.

Appendix 2:

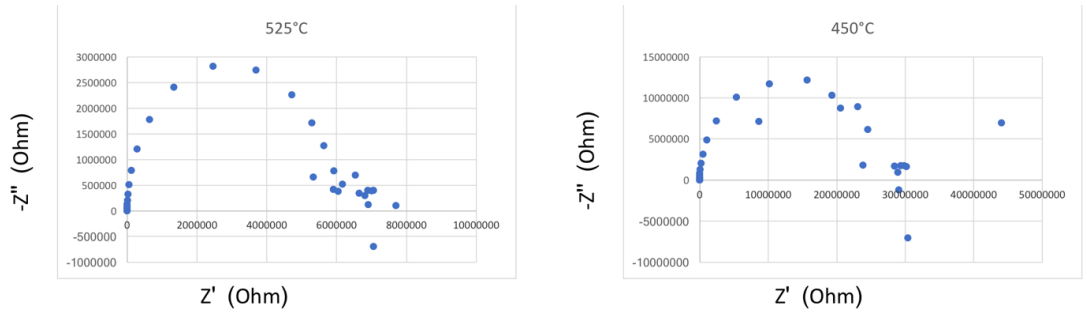

Figure: Impedance analyses of 10%Na_2CO_3-90%TiO_2 (reduced at 700°C-0.5 hours) taken at 525°C and 450°C.

Appendix 3:

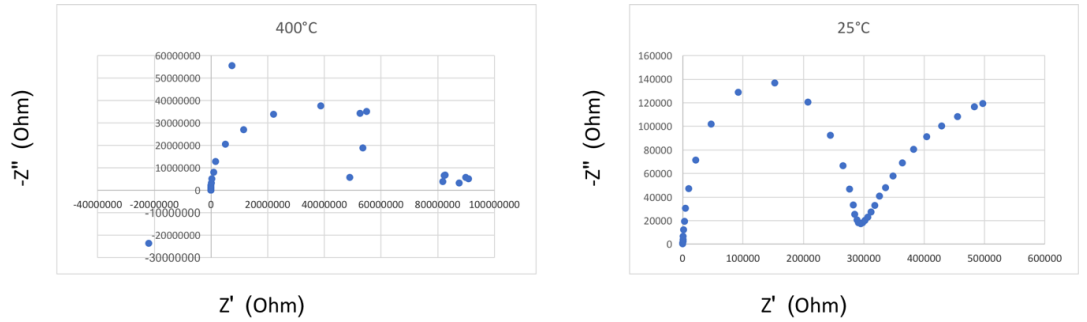

Figure: Impedance analyses of 10%Na_2CO_3-90%TiO_2 (reduced at 700°C-0.5 hours) taken at 400°C and 25°C.

Appendix 4:

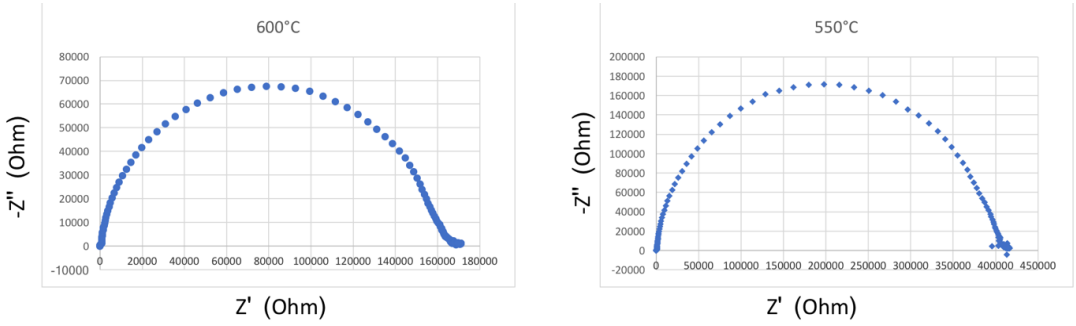

Figure: Impedance analyses of 10%Na_2CO_3-90%TiO_2 (reduced at 700°C-4 hours) taken at 600°C and 550°C.

Appendix 5:

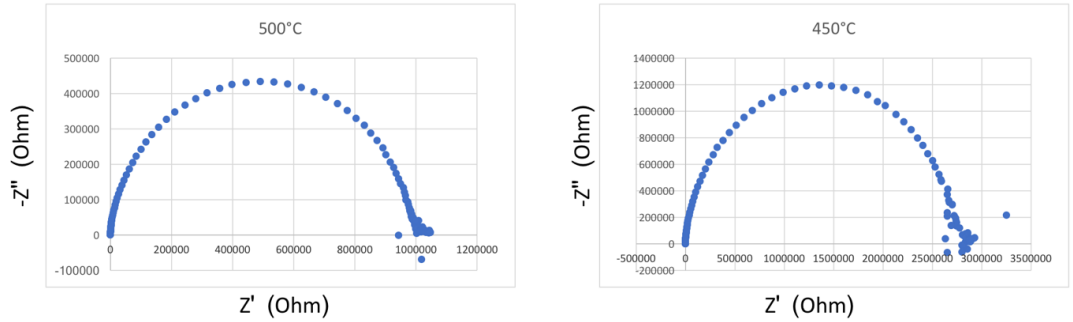

Figure: Impedance analyses of 10%Na_2CO_3-90%TiO_2 (reduced at 700°C-4 hours) taken at 500°C and 450°C.

Appendix 6:

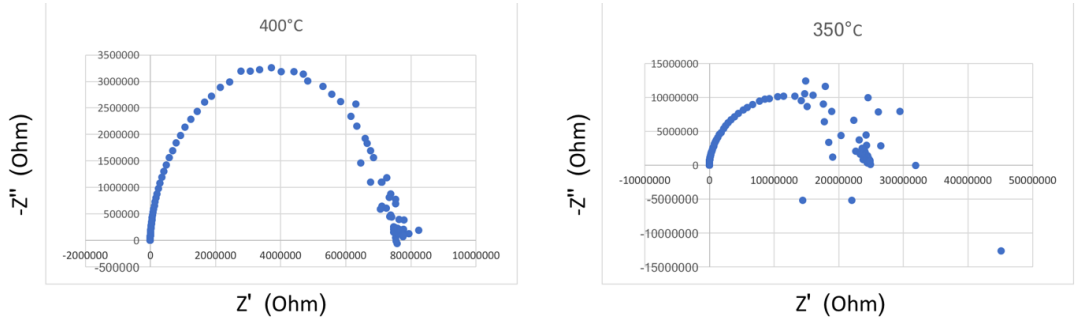

Figure: Impedance analyses of 10%Na_2CO_3-90%TiO_2 (reduced at 700°C-4 hours) taken at 400°C and 350°C.

Appendix 7:

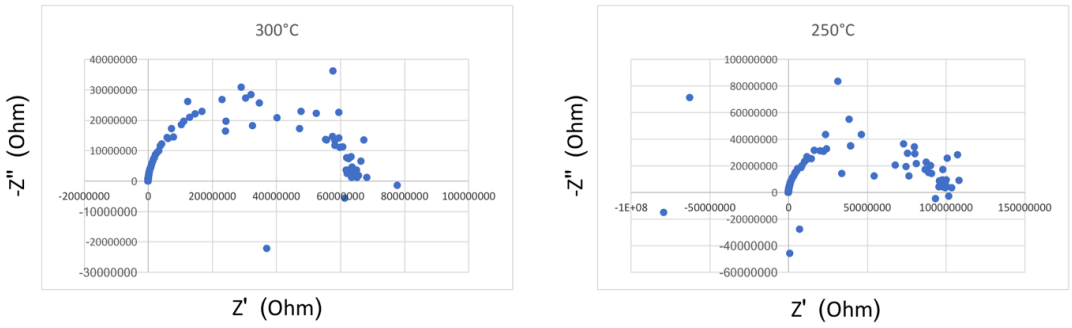

Figure: Impedance analyses of 10%Na_2CO_3-90%TiO_2 (reduced at 700°C-4 hours) taken at 300°C and 250°C.

Appendix 8:

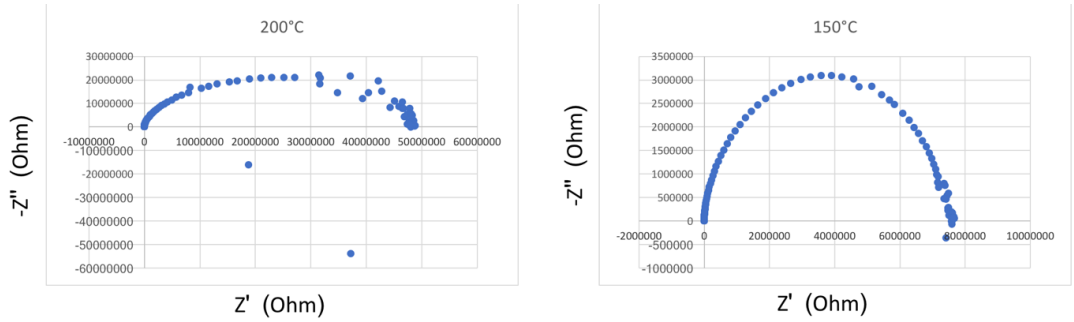

Figure: Impedance analyses of 10%Na_2CO_3-90%TiO_2 (reduced at 700°C-4 hours) taken at 200°C and 150°C.

Appendix 9:

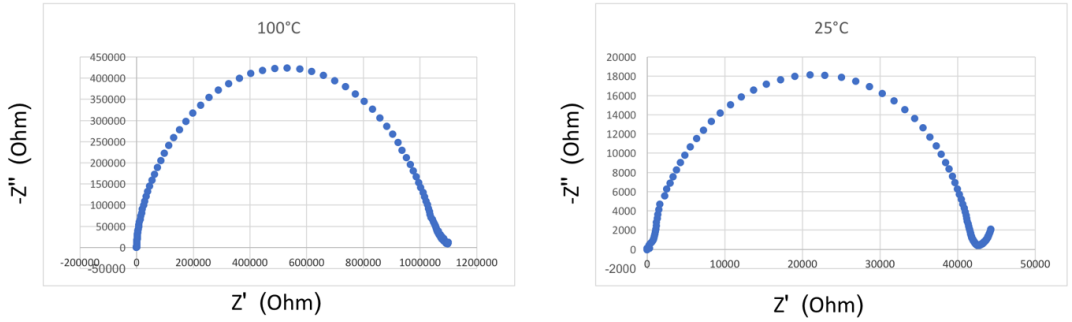

Figure: Impedance analyses of 10%Na_2CO_3-90%TiO_2 (reduced at 700°C-4 hours) taken at 100°C and 25°C.

Appendix 10:

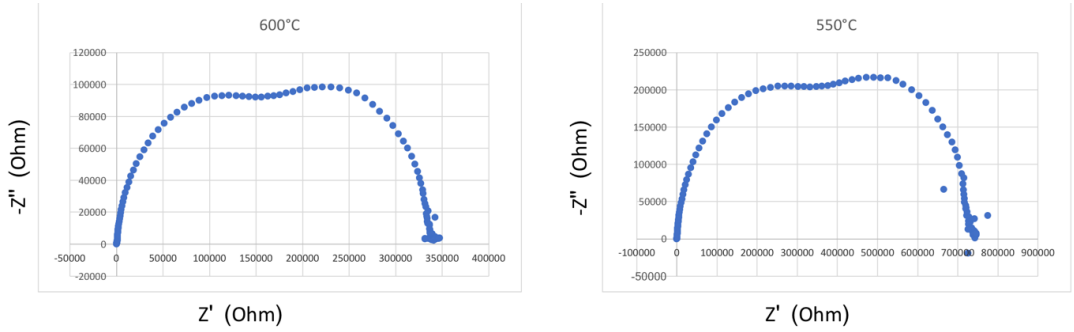

Figure: Impedance analyses of 10%Na_2CO_3-90%TiO_2 (reduced at 800°C-4 hours) taken at 600°C and 550°C.

Appendix 11:

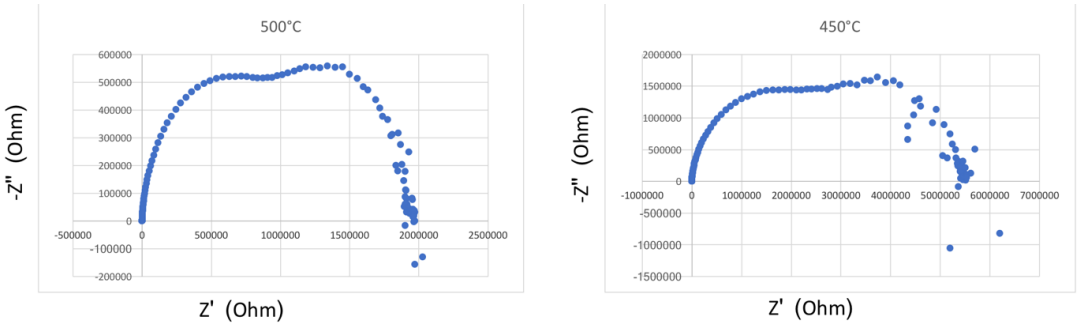

Figure: Impedance analyses of 10%Na_2CO_3-90%TiO_2 (reduced at 800°C-4 hours) taken at 500°C and 450°C.

Appendix 12:

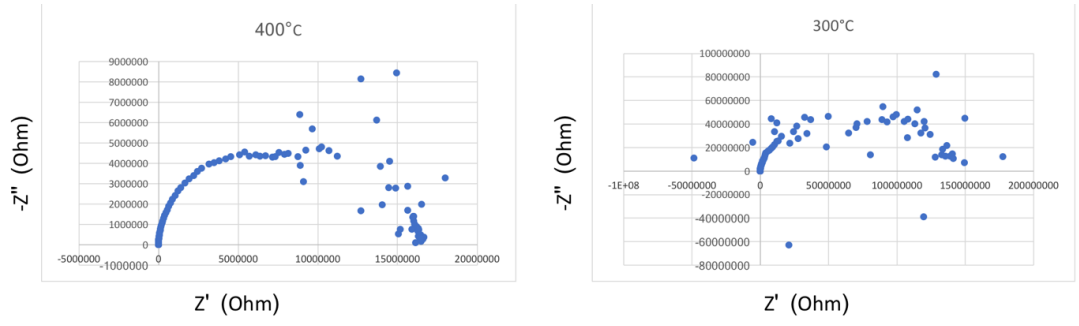

Figure: Impedance analyses of 10%Na_2CO_3-90%TiO_2 (reduced at 800°C-4 hours) taken at 400°C and 300°C.

Appendix 13:

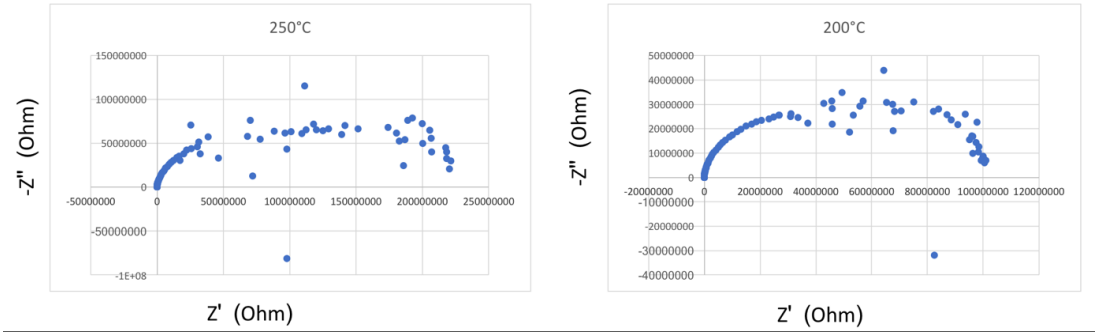

Figure: Impedance analyses of 10%Na_2CO_3-90%TiO_2 (reduced at 800°C-4 hours) taken at 250°C and 200°C.

Appendix 14:

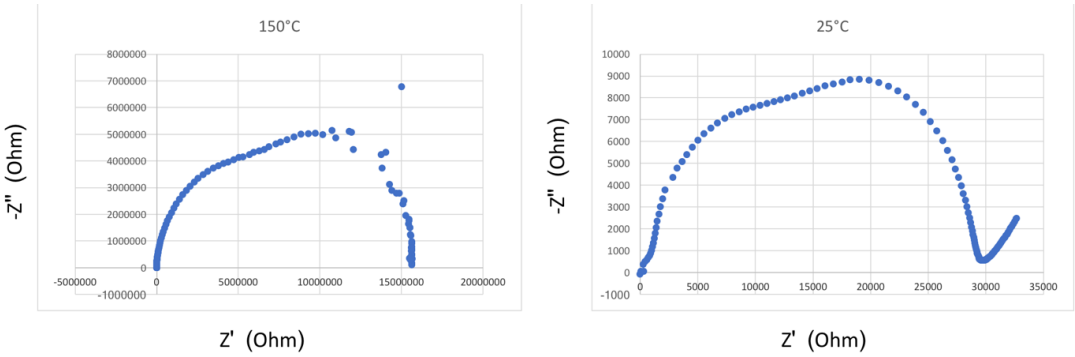

Figure: Impedance analyses of 10%Na_2CO_3-90%TiO_2 (reduced at 800°C-4 hours) taken at 150°C and 25°C.

Appendix 15:

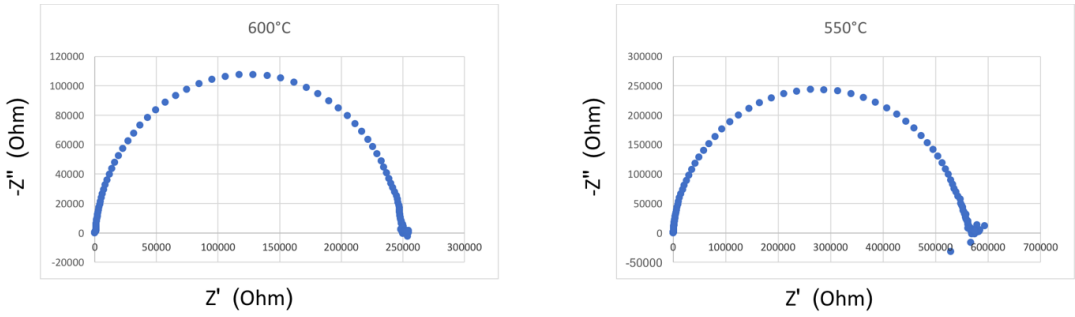

Figure: Impedance analyses of 10%Na_2CO_3-90%TiO_2 (reduced at 850°C-4 hours) taken at 600°C and 550°C.

Appendix 16:

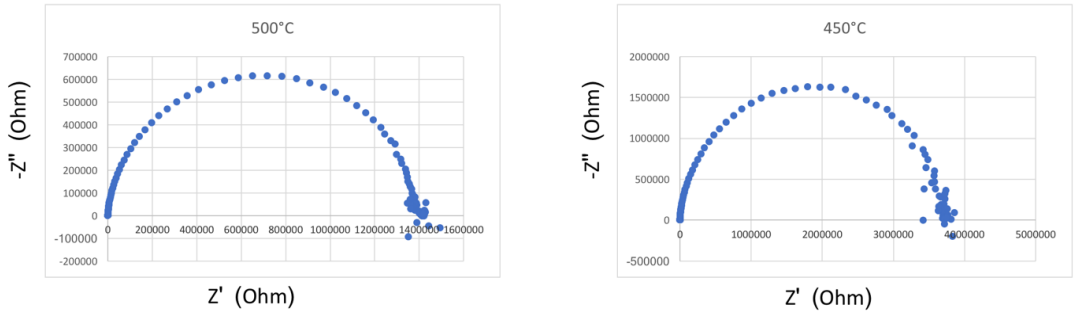

Figure: Impedance analyses of 10%Na_2CO_3-90%TiO_2 (reduced at 850°C-4 hours) taken at 500°C and 450°C.

Appendix 17:

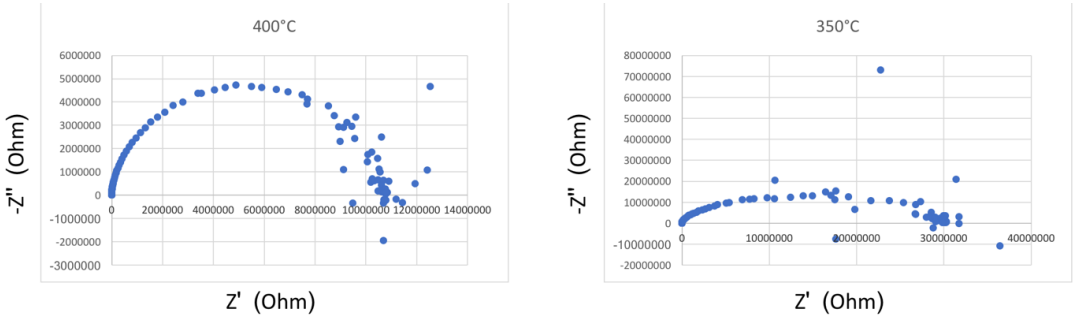

Figure: Impedance analyses of 10%Na_2CO_3-90%TiO_2 (reduced at 850°C-4 hours) taken at 400°C and 350°C.

Appendix 18:

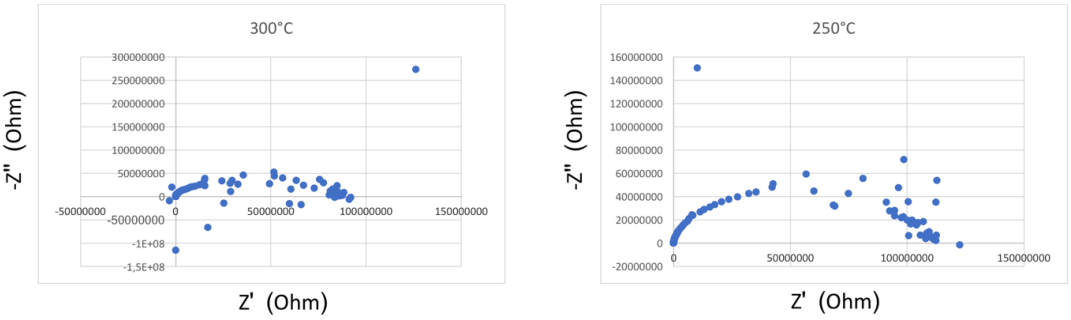

Figure: Impedance analyses of 10%Na_2CO_3-90%TiO_2 (reduced at 850°C-4 hours) taken at 300°C and 250°C.

Appendix 19:

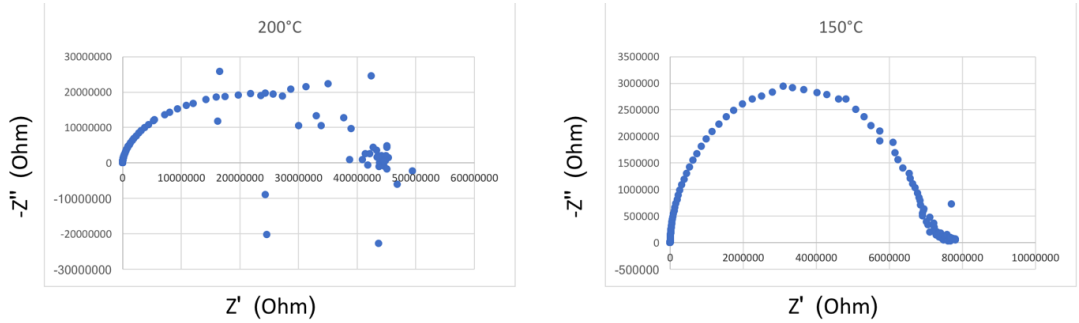

Figure: Impedance analyses of 10%Na_2CO_3-90%TiO_2 (reduced at 850°C-4 hours) taken at 200°C and 150°C.

Appendix 20:

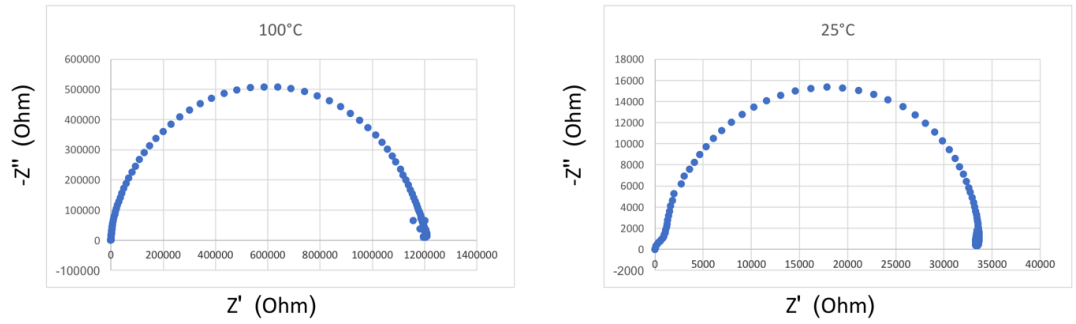

Figure: Impedance analyses of 10%Na_2CO_3-90%TiO_2 (reduced at 850°C-4 hours) taken at 100°C and 25°C.

Appendix 21:

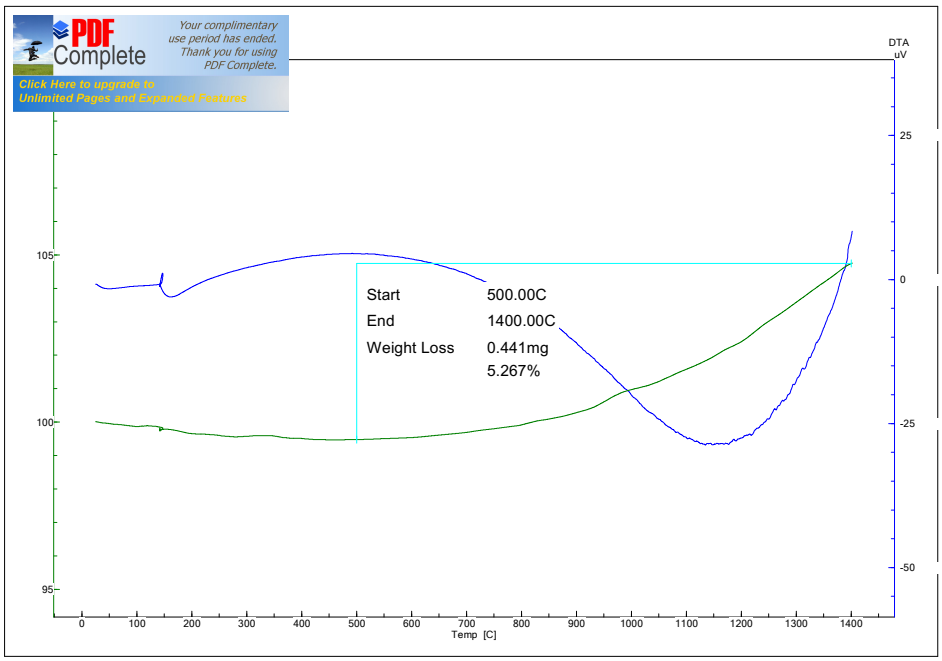

Figure: Thermal analysis of TiO_2 powder reduced at 700 ^oC for 0.5 hours.

Appendix 22:

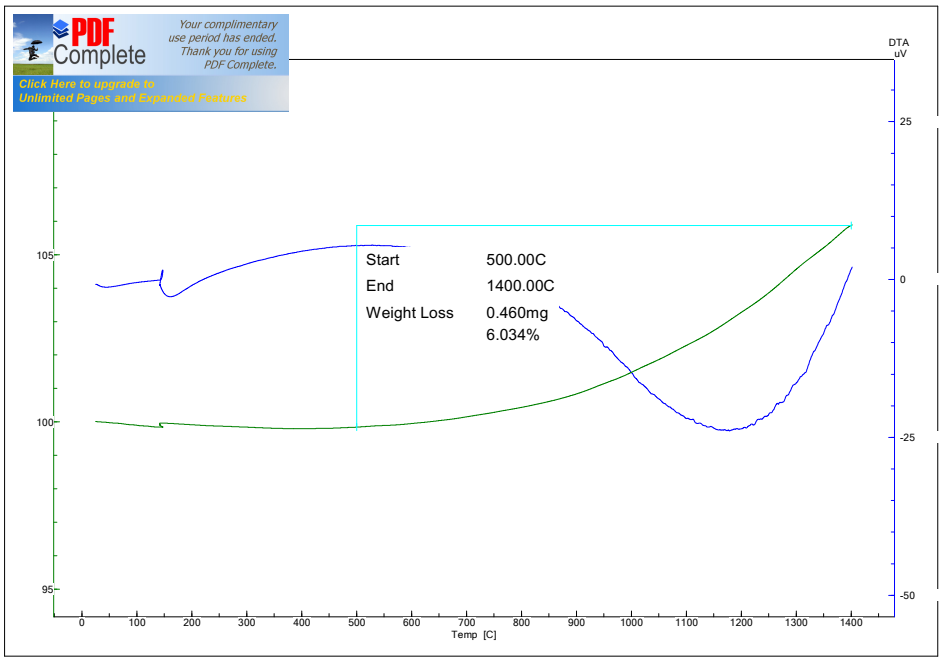

Figure: Thermal analysis of TiO_2 powder reduced at 700 ^oC for 4 hours.

Appendix 23:

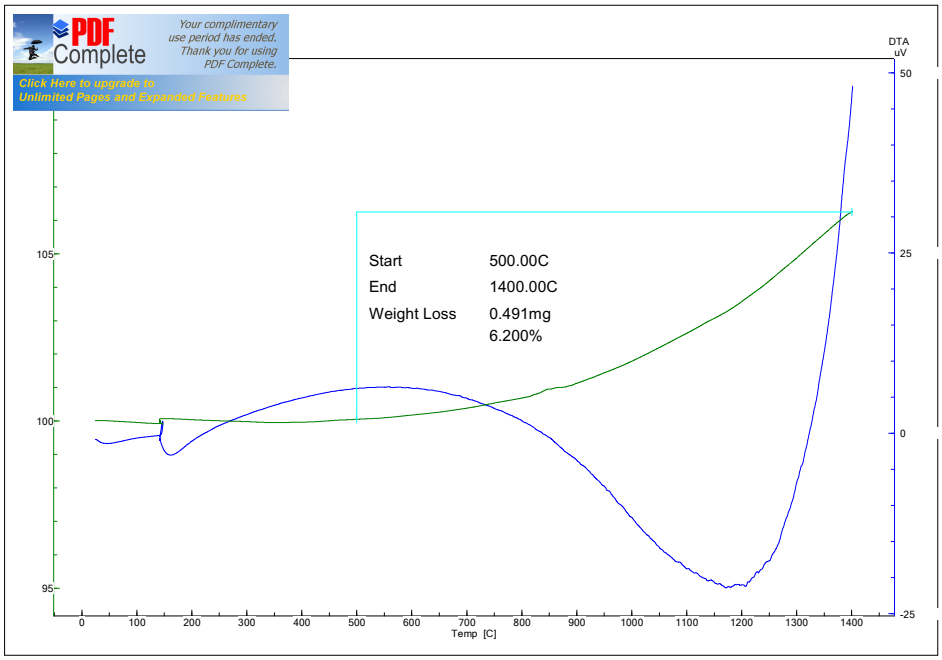

Figure: Thermal analysis of TiO_2 powder reduced at 800 ^oC for 4 hours.

Appendix 24:

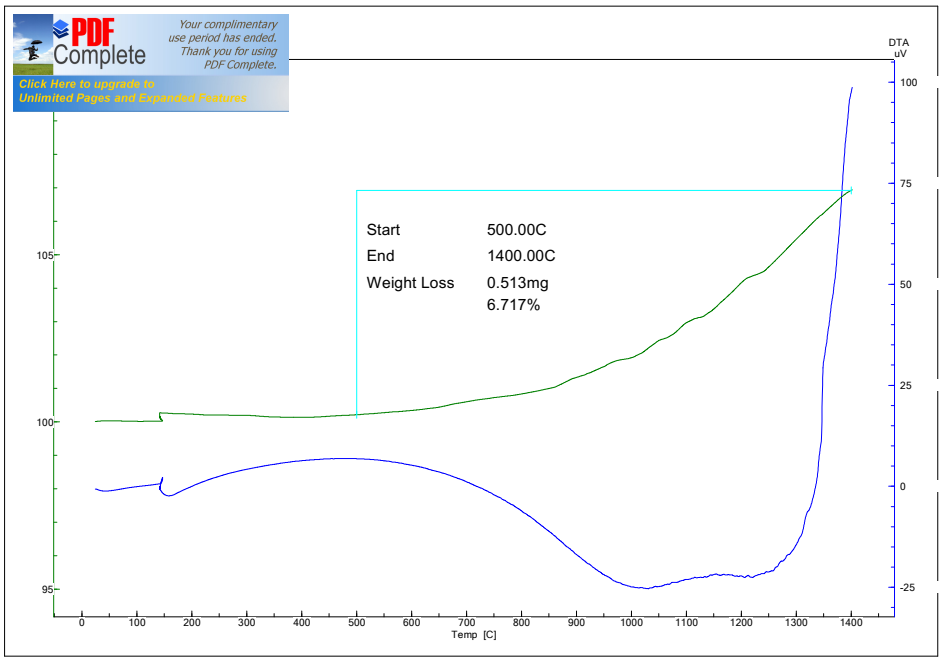

Figure: Thermal analysis of TiO_2 powder reduced at 800 ^oC for 4 hours with addition of graphite powder to the system.

Appendix 25:

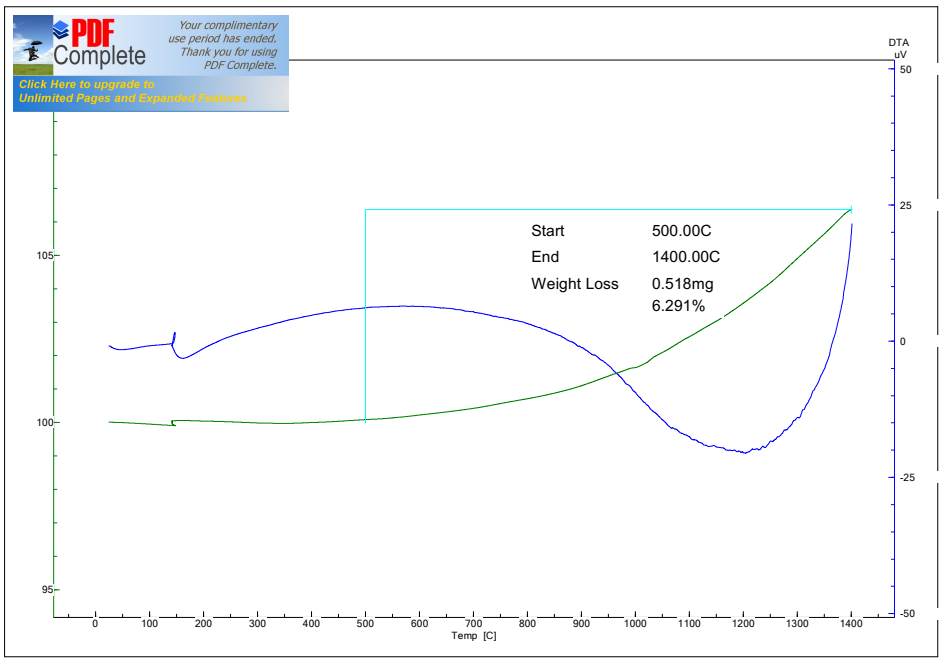

Figure: Thermal analysis of TiO_2 powder reduced at 850 ^oC for 4 hours.

Appendix 26:

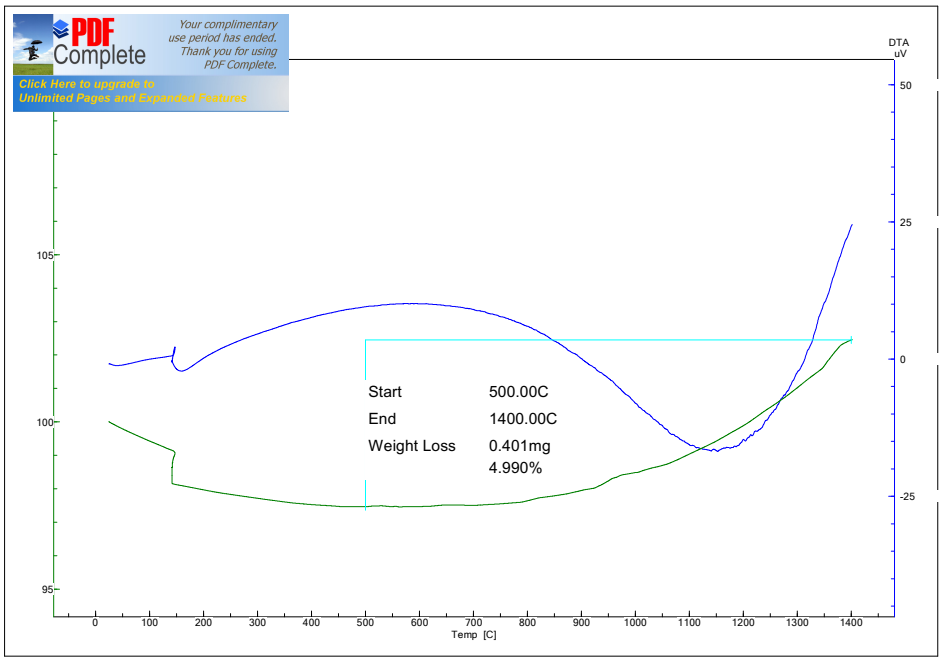

Figure: Thermal analysis of TiO_2 powder reduced at 900 ^oC for 4 hours.

Appendix 27:

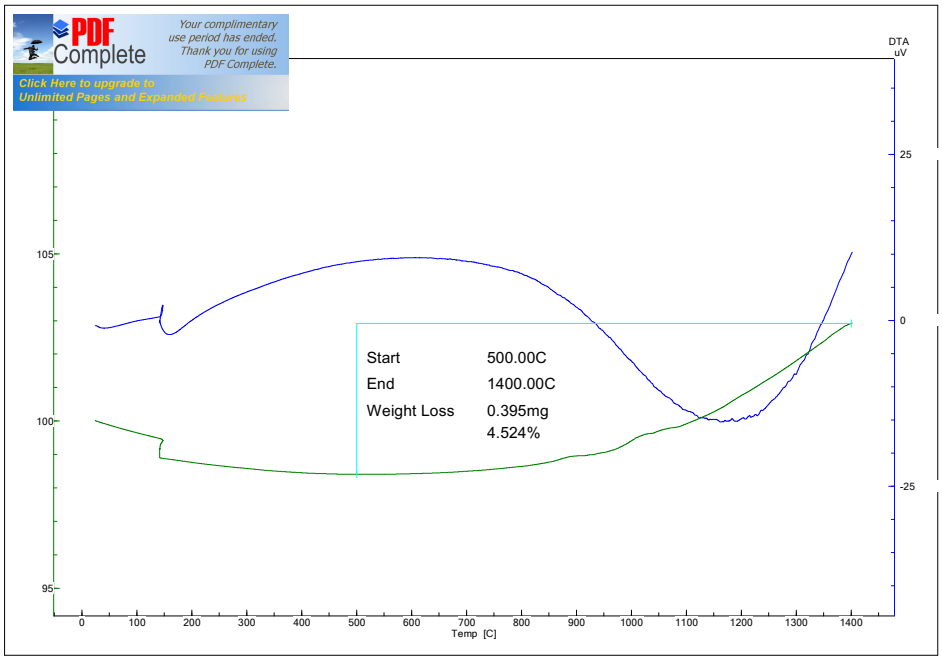

Figure: Thermal analysis of TiO_2 powder reduced at 1000 ^oC for 4 hours.

Appendix 28:

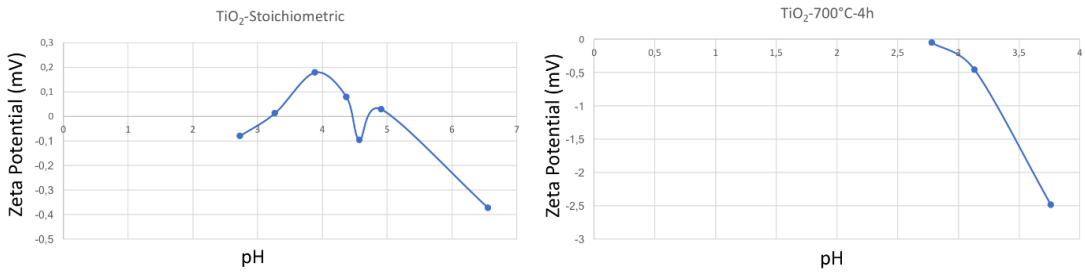

Figure: Isoelectric point measurements for as received TiO_2 and TiO_2 reduced at 700 °C for 4 hours.

Appendix 29:

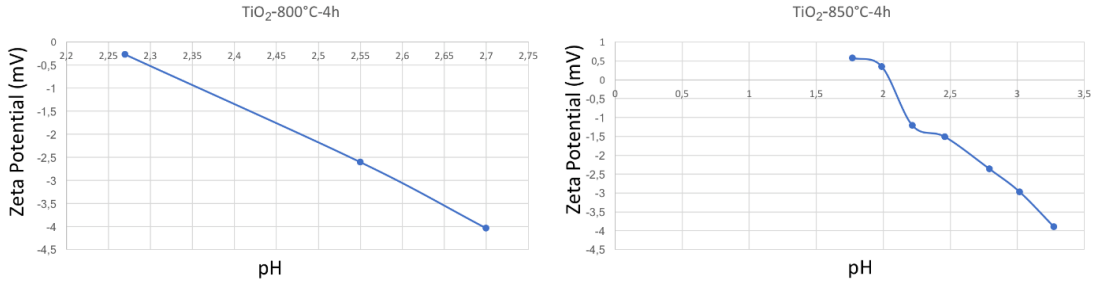

Figure: Isoelectric point measurements for TiO_2 reduced at 800 °C and 850 °C for 4 hours.

Appendix 30:

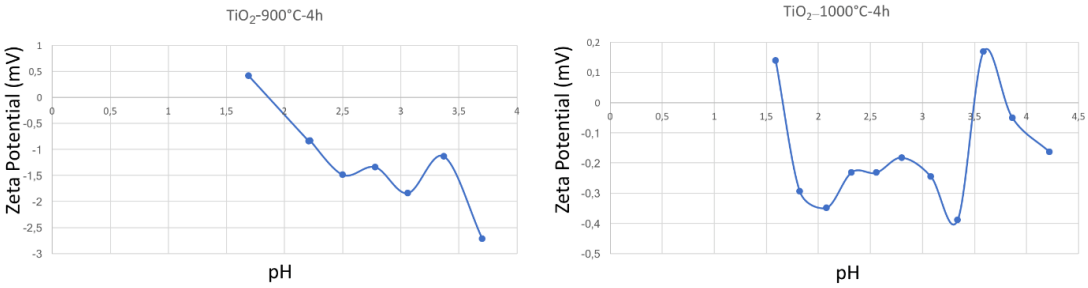

Figure: Isoelectric point measurements for TiO_2 reduced at 900 °C and 1000 °C for 4 hours.

Appendix 31:

Table: Isoelectric point measurements with auto-titration.

Powder Type	IEP
TiO_2 (As received)	3.20, 4.46, 4.83, 5.02

TiO_2 reduced at 700 °C for 4 hours	2.85
TiO_2 reduced at 800 °C for 4 hours	2.24
TiO_2 reduced at 800 °C for 4 hours-Graphite	2.40
TiO_2 reduced at 850 °C for 4 hours	2.04
TiO_2 reduced at 900 °C for 4 hours	1.86
TiO_2 reduced at 1000 °C for 4 hours	1.67, 3.51, 3.80

Appendix 32:

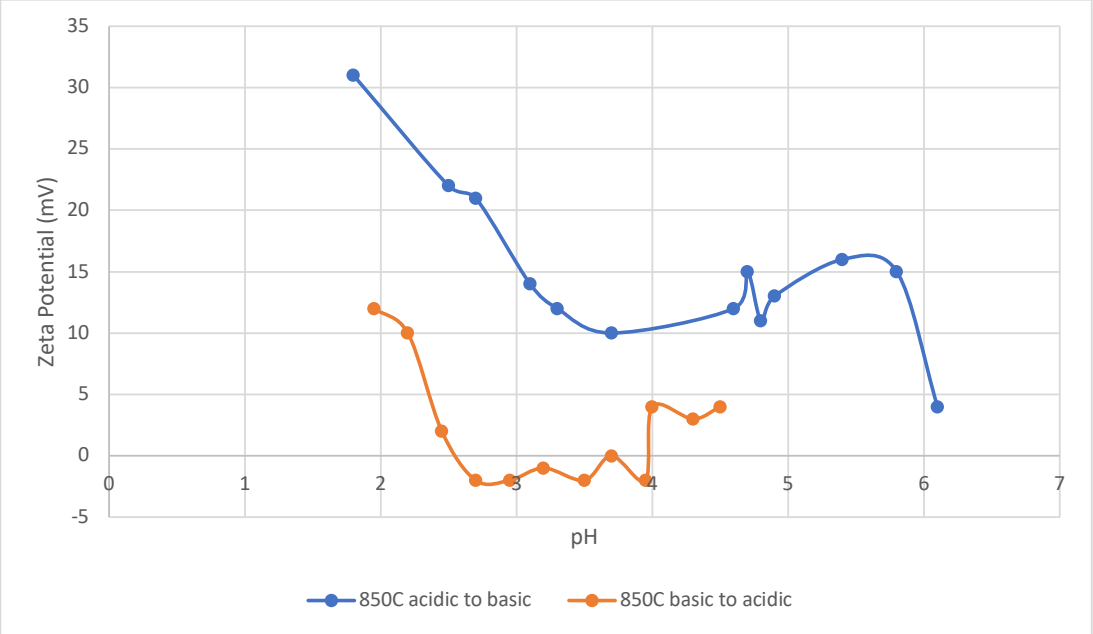

Figure: Zeta potential study of TiO_2 reduced at 850 °C for 4 hours with auto-titration depending on starting pH values.

Appendix 33:

Gmail **deniz benli <denizbnli@gmail.com>**

Thank you for your order with RightsLink / John Wiley and Sons
1 message

no-reply@copyright.com <no-reply@copyright.com> Fri, Feb 1, 2019 at 1:19 PM
To: denizbnli@gmail.com

WILEY

Thank you for your order!

Dear Mr. Ahmet Deniz Benli,

Thank you for placing your order through Copyright Clearance Center's RightsLink® service.

Order Summary

Licensee:	Mr. Ahmet Deniz Benli
Order Date:	Feb 1, 2019
Order Number:	4520121001433
Publication:	Wiley Books
Title:	Physical Ceramics: Principles for Ceramic Science and Engineering
Type of Use:	Dissertation/Thesis
Order Total:	0.00 USD

View or print complete details of your order and the publisher's terms and conditions.

Sincerely,

Copyright Clearance Center

Tel: +1-855-239-3415 / +1-978-646-2777
customercare@copyright.com
https://myaccount.copyright.com

Copyright Clearance Center RightsLink®

JOHN WILEY AND SONS LICENSE TERMS AND CONDITIONS

Feb 04, 2019

This Agreement between Mr. Ahmet Deniz Benli ("You") and John Wiley and Sons ("John Wiley and Sons") consists of your license details and the terms and conditions provided by John Wiley and Sons and Copyright Clearance Center.

License Number	4520121001433
License date	Feb 01, 2019
Licensed Content Publisher	John Wiley and Sons
Licensed Content Publication	Wiley Books
Licensed Content Title	Physical Ceramics: Principles for Ceramic Science and Engineering
Licensed Content Author	Dunbar P. Birnie W. David Kingery Yet-Ming Chiang
Licensed Content Date	May 1, 1996
Licensed Content Pages	1
Type of use	Dissertation/Thesis
Requestor type	University/Academic
Format	Print and electronic
Portion	Figure/table
Number of figures/tables	1
Original Wiley figure/table number(s)	Figure 2.24
Will you be translating?	No
Title of your thesis / dissertation	Nanocomposite Fuel Cells
Expected completion date	Feb 2019
Expected size (number of pages)	64
Requestor Location	Mr. Ahmet Deniz Benli Sabancı University Istanbul, 34956 Turkey Attn: Mr. Ahmet Deniz Benli
Publisher Tax ID	EU826007151
Total	0.00 USD
Terms and Conditions	

TERMS AND CONDITIONS

This copyrighted material is owned by or exclusively licensed to John Wiley & Sons, Inc. or one of its group companies (each a"Wiley Company") or handled on behalf of a society with which a Wiley Company has exclusive publishing rights in relation to a particular work (collectively "WILEY"). By clicking "accept" in connection with completing this licensing transaction, you agree that the following terms and conditions apply to this transaction (along with the billing and payment terms and conditions established by the Copyright Clearance Center Inc., ("CCC's Billing and Payment terms and conditions"), at the time that you opened your RightsLink account (these are available at any time at http://myaccount.copyright.com).